determined by RIA using rabbit anti-Ang I antiserum and rabbit anti-Ang II antiserum (Arnel Inc.) as previously reported (33).

Real-time quantitative RT-PCR analysis. We extracted total RNA from part of the kidney removed from each animal by using an RNeasy Mini Kit (QIAGEN KK) and performed a real-time quantitative RT-PCR by using the TaqMan One-Step RT-PCR Master Mix Reagents Kit with an ABI Prism 7700 HT Detection System (Applied Biosystems Inc.) and probes and primers for the rat genes encoding the following: renin (forward, 5′-GCTACATGGAGAATGGGACTGAA-3′; reverse, 5′-ACCACATCTTGGCTGAGGAAAC-3′; probe, 5′-FAM-CCATCCACTATGGATCAGGGAAGGTCAA-TAMRA-3′); ACE (forward, 5′-CTGCCTCCCAACGAGTTAGAA-3′; reverse, 5′-CGGGACGTGGCCATTATATT-3′; probe, 5′-FAM-AAATGGCACTTGTCTGTCACTGGAGCCTAMRA-3′); angiotensinogen (forward, 5′-AGCACGGACAGCACCCTATT-3′; reverse, 5′-AGAACTCATGGAGCCCAGTCA-3′; probe, 5′-FAM-TCAACACCTACGTTCACTTCCAAGGGAAGA-TAMRA-3′); cathepsin B (forward, 5′-AAATCAGGCGTATACAAGCATGA-3′; reverse, 5′-GCCCAGAATGCGGATGG-3′; probe, 5′-FAM-CCGGTGATGTGATGGGAGGCCA-TAMRA-3′); and GAPDH (forward, 5′-TGACAACTCCCTCAAGATTGTCA-3′; reverse, 5′-GGCATGGACTGTGGTCATGA-3′; probe, 5′-FAM-TGCATCCTGCACCACCAACTGCTTAG-TAMRA-3′); as described previously (34, 35).

Statistical analyses. Within-group statistical comparisons were made by one-way ANOVA for repeated measures followed by the Newman-Keuls post hoc test. Differences between two groups were evaluated by two-way ANOVA for repeated measures combined with the Newman-Keuls post-hoc test. A P value of less than 0.05 was considered significant. Data are reported as means ± SEM.

Acknowledgments

This work was supported in part by grants 14571073, 1503340, and 16613002 from the Ministry of Education, Science, and Culture of Japan; a grant from the Takeda Science Foundation (to A. Ichihara); NIH research grant HL-58205; and Health and Labour Sciences Research Grants, Research on Measures for Intractable Diseases, from the Ministry of Health, Labour, and Welfare of Japan. We thank Rika Wakita for her dedicated attention to the many details involved in the preparation of this paper.

Received for publication February 23, 2004, and accepted in revised form August 24, 2004.

Address correspondence to: Atsuhiro Ichihara, Department of Internal Medicine, Keio University School of Medicine, 35 Shinanomachi, Shinjuku-ku, Tokyo, 160-8582, Japan. Phone: 81-3-5363-3796; Fax: 81-3-3359-2745; E-mail: atzichi@sc.itc.keio.ac.jp.

1. Luetscher, J.A., Kraemer, F.B., Wilson, D.M., Schwartz, H.C., and Bryer-Ash, M. 1985. Increased plasma inactive renin in diabetes mellitus: a marker of microvascular complications. *N. Engl. J. Med.* 312:1412–1417.
2. Deinum, J., et al. 1999. Increase in serum prorenin precedes onset of microalbuminuria in patients with insulin-dependent diabetes mellitus. *Diabetologia.* 42:1006–1010.
3. Véniant, M., et al. 1996. Vascular damage without hypertension in transgenic rats expressing prorenin exclusively in the liver. *J. Clin. Invest.* 98:1966–1970.
4. Peters, J., et al. 2002. Functional significance of prorenin internalization in the rat heart. *Circ. Res.* 90:1135–1141.
5. Suzuki, F., et al. 2003. Human prorenin has "gate and handle" regions for its non-proteolytic activation. *J. Biol. Chem.* 278:22217–22222.
6. Maru, I., Ohta, Y., Murata, K., and Tsukada, Y. 1996. Molecular cloning and identification of N-acyl-D-glucosamine 2-epimerase from porcine kidney as a renin-binding protein. *J. Biol. Chem.* 271:16294–16299.
7. Van-Kesteren, C.A.M., et al. 1997. Mannose 6-phosphate receptor-mediated internalization and activation of prorenin by cardiac cells. *Hypertension.* 30:1389–1396.
8. Admiraal, P.J.J., et al. 1999. Uptake and proteolytic activation of prorenin by cultured human endothelial cells. *J. Hypertens.* 17:621–629.
9. Nguyen, G., et al. 2002. Pivotal role of the renin/prorenin receptor in angiotensin II production and cellular responses to renin. *J. Clin. Invest.* 109:1417–1427. doi:10.1172/JCI200214276.
10. deCavanagh, E.M.V., et al. 2001. Enalapril attenuates oxidative stress in diabetic rats. *Hypertension.* 38:1130–1136.
11. Onozato, M.L., Tojo, A., Goto, A., Fujita, T., and Wilcox, C.S. 2002. Oxidative stress and nitric oxide synthase in rat diabetic nephropathy: effects of ACEI and ARB. *Kidney Int.* 61:186–194.
12. Hayashi, M., Senba, S., Saito, I., Kitajima, W., and Saruta, T. 1983. Changes in blood pressure, urinary kallikrein, and urinary prostaglandin E2 in rats with streptozotocin-induced diabetes. *Naunyn Schmiedebergs Arch. Pharmacol.* 322:290–294.
13. Zimpelmann, J., et al. 2000. Early diabetes mellitus stimulates proximal tubule renin mRNA expression in the rat. *Kidney Int.* 58:2320–2330.
14. Vallon, V., Wead, L.M., and Blantz, R.C. 1995. Renal hemodynamics and plasma and kidney angiotensin II in established diabetes mellitus in rats: effect of sodium and salt restriction. *J. Am. Soc. Nephrol.* 5:1761–1767.
15. Kennefick, T.M., Oyama, T.T., Thompson, M.M., Vora, J.P., and Anderson, S. 1996. Enhanced renal sensitivity to angiotensin actionc in diabetes mellitus in the rat. *Am. J. Physiol.* 271:F595–F602.
16. Campbell, D.J., Kelly, D.J., Wilkinson-Berka, J.L., Cooper, M.E., and Skinner, S.L. 1999. Increased bradykinin and "normal" angiotensin peptide levels in diabetic Sprague-Dawley and transgenic (mRen-2)27 rats. *Kidney Int.* 56:211–221.
17. Everett, A.D., et al. 1992. Renin and angiotensinogen expression during the evolution of diabetes. *Hypertension.* 19:70–78.
18. Kalinyak, J.E., et al. 1993. The renin-angiotensin system in streptozotocin-induced diabetes mellitus in the rat. *J. Am. Soc. Nephrol.* 4:1337–1345.
19. Choi, K.C., et al. 1997. Alterations of intrarenal renin-angiotensin and nitric oxide systems in streptozotocin-induced diabetic rats. *Kidney Int. S2*(Suppl.):S23–S27.
20. Zhang, S.-L., et al. 1999. Molecular mechanisms of glucose action on angiotensinogen gene expression in rat proximal tubular cells. *Kidney Int. 55*:454–464.
21. Anderson, S., Jung, F.F., and Ingelfinger, J.R. 1993. Renal renin-angiotensin system in diabetes: functional, immunohistochemical, and molecular biological correlations. *Am. J. Physiol. 265*:F477–F486.
22. Leehey, D.J., Song, R.H., Alavi, N., and Singh, A.K. 1995. Decreased degradative enzymes in mesangial cells cultured in high glucose media. *Diabetes.* 44:929–935.
23. Song, R.H., Singh, A.K., and Leehey, D.J. 1999. Decreased glomerular proteinase activity in the streptozotocin diabetic rat. *Am. J. Nephrol.* 19:441–446.
24. Lewis, E.J., et al. 2001. Renoprotective effect of the angiotensin-receptor antagonist irbesartan in patients with nephropathy due to type 2 diabetes. *N. Engl. J. Med.* 345:851–860.
25. Brenner, B.M., et al. 2001. Effects of losartan on renal and cardiovascular outcomes in patients with type 2 diabetes and nephropathy. *N. Engl. J. Med.* 345:861–869.
26. Takii, Y., Figueiredo, A.F.S., and Inagami, T. 1985. Application of immunochemical methods to the identification and characterization of rat kidney inactive renin. *Hypertension.* 7:236–243.
27. El-Nahas, A.M., Bassett, A.H., Cope, G.H., and Carpentier, J.E. 1991. Role of growth hormone in the development of experimental renal scarring. *Kidney Int.* 40:29–34.
28. Kalluri, R., Shield, C.F., Todd, P., Hudson, B.G., and Neilson, E.G. 1997. Isoform switching of type IV collagen is developmentally arrested in X-linked Alport syndrome leading to increased susceptibility of renal basement membranes to endoproteolysis. *J. Clin. Invest.* 99:2470–2478.
29. Inagami, T., Murakami, T., Higuchi, K., and Nakajo, S. 1991. Roles of renal and vascular renin in spontaneous hypertension and switching of the mechanism upon nephrectomy. *Am. J. Hypertens.* 4:1SS–22S.
30. Iwai, N., Inagami, T., Ohmichi, N., and Kinoshita, M. 1996. Renin is expressed in rat macrophage/monocyte cells. *Hypertension.* 27:399–403.
31. Hirota, N., Ichihara, A., Koura, Y., Hayashi, M., and Saruta, T. 2002. Phospholipase D contributes to transmural pressure control of prorenin processing in juxtaglomerular cell. *Hypertension.* 39:363–367.
32. Kobori, H., et al. 1997. Thyroid hormone stimulates renin synthesis in rats without involving the sympathetic nervous system. *Am. J. Physiol.* 272:E227–E232.
33. Nishiyama, A., Seth, D.M., and Navar, L.G. 2002. Renal interstitial fluid angiotensin I and angiotensin II concentrations during local angiotensin-converting enzyme inhibition. *J. Am. Soc. Nephrol.* 13:2207–2212.
34. Naito, Y., Tsujino, T., Fujioka, Y., Ohyanagi, M., and Iwasaki, T. 2002. Augmented diurnal variations of the cardiac renin-angiotensin system in hypertensive rats. *Hypertension.* 40:827–833.
35. Wasselius, J., Wallin, H., Abrahamson, M., and Ehinger, B. 2003. Cathepsin B in the rat eye. *Graefe's Arch. Clin. Exp. Ophthalmol.* 241:934–942.

ELSEVIER

Mechanisms of Development 121 (2004) 547–557

www.elsevier.com/locate/modo

Identification of kidney mesenchymal genes by a combination of microarray analysis and *Sall1-GFP* knockin mice☆

Minoru Takasato[a,b], Kenji Osafune[a,c], Yuko Matsumoto[a], Yuki Kataoka[d], Nobuaki Yoshida[d], Hiroko Meguro[e], Hiroyuki Aburatani[e], Makoto Asashima[b,c], Ryuichi Nishinakamura[a,f,g,*]

[a]*Division of Stem Cell Regulation, The Institute of Medical Science, The University of Tokyo, 4-6-1 Minato-ku Shirokanedai, Tokyo 108-8639, Japan*
[b]*Department of Biological Sciences, Graduate School of Science, The University of Tokyo, Tokyo 113-8654, Japan*
[c]*Department of Life Sciences (Biology), Graduate School of Art and Sciences, The University of Tokyo, Tokyo 153-8902, Japan*
[d]*Laboratory of Gene Expression and Regulation, The Institute of Medical Science, The University of Tokyo, Tokyo 108-8639, Japan*
[e]*Genome Science Division, Research Center for Advanced Science and Technology, The University of Tokyo, Tokyo 153-8904, Japan*
[f]*Division of Integrative Cell Biology, Institute of Molecular Embryology and Genetics, Kumamoto University, Kumamoto 860-0811, Japan*
[g]*PREST, JST, Saitama 332-0012, Japan*

Received 7 November 2003; received in revised form 8 March 2004; accepted 7 April 2004

Available online 22 April 2004

Abstract

SALL1, a causative gene for Townes-Brocks syndrome, encodes a zinc finger protein, and its mouse homolog (*Sall1*) is essential for metanephros development, as noted during gene targeting. In the embryonic kidney, *Sall1* is expressed abundantly in mesenchyme-derived structures from condensed mesenchyme, S-, comma-shaped bodies, to renal tubules and podocytes. We generated mice in which a green fluorescent protein (*GFP*) gene was inserted into the *Sall1* locus and we isolated the *GFP*-positive population from embryonic kidneys of these mice by fluorescein-activated cell sorting. The *GFP*-positive population indeed expressed mesenchymal genes, while the negative population expressed genes in the ureteric bud. To systematically search for genes expressed in the mesenchyme-derived cells, we compared gene expression profiles in the *GFP*-positive and -negative populations using microarray analysis, followed by in situ hybridization. We detected many genes known to be important for metanephros development including *Sall1, GDNF, Raldh2, Pax8* and *FoxD1*, and genes expressed abundantly in the metanephric mesenchyme such as *Unc4.1, Six2, Osr-2* and *PDGFc*. We also found groups of genes including *SSB-4, Smarcd3, μ-Crystallin, TRB-2*, which are not known to be expressed in the metanephric mesenchyme. Therefore a combination of microarray technology and *Sall1-GFP* mice is useful for systematic identification of genes expressed in the developing kidney.

Keywords: Kidney development; Microarray; *Sall1*; Knockin; Fluorescein-activated cell sorting; Metanephric mesenchyme

1. Introduction

In the mammalian kidney there are stromal cells, glomeruli, proximal and distal tubules, loops of Henle and collecting ducts, but all these components originate from only two types of tissues, epithelium of the ureteric bud and the metanephric mesenchyme. Around E11 in mice, the metanephric mesenchyme induces the ureteric bud to invade the metanephric mesenchyme and branch. Upon reciprocal induction by the ureteric bud, the mesenchymal cells aggregate and form blastema around the ureteric bud. The blastema develops into epithelial cells that form the nephron. The region of the metanephric mesenchyme diminishes gradually until 7 days after birth, and kidney development is complete when the metanephric mesenchyme disappears. Metanephric mesenchymal cells differentiate into at least three distinct cell types; glomerular, proximal and distal tubule epithelia as noted in retroviral mediated *lac-Z* gene transfer assay (Herzlinger et al., 1992), demonstrating that the metanephric mesenchyme represents multipotent progenitor cells of the nephron.

☆ Supplementary data associated with this article can be found, in the online version, at doi = 10.1016/j.mod.2004.04.007.

* Corresponding author. Address: Division of Integrative Cell Biology, Institute of Molecular Embryology and Genetics, Kumamoto University, 2-2-1 Honjo, Kumamoto 860-0811, Japan. Tel.: +81-96-373-6615; fax: +81-96-373-6618.

E-mail address: ryuichi@kaiju.medic.kumamoto-u.ac.jp (R. Nishinakamura).

0925-4773/$ - see front matter © 2004 Elsevier Ireland Ltd. All rights reserved.
doi:10.1016/j.mod.2004.04.007

Molecular mechanisms of kidney development have been determined mostly by gene targeting, and many mesenchymal genes including *WT1*, *Eya1*, *GDNF* and *Six1* are known to have important roles in kidney development. The transcription factor *WT1* is first expressed in the metanephric mesenchyme before induction, and in *WT1* null mutant mice the ureter never reaches the mesenchyme and consequently the mesenchyme undergoes apoptosis (Kreidberg et al., 1993). The transcriptional coactivator *Eya1* is only expressed in the metanephric mesenchyme and *Eya1* $-/-$ mice show renal agenesis and their posterior intermediate mesoderm fails to produce the glial-derived neurotrophic factor (*GDNF*) (Xu et al., 1999; Buller et al., 2001). *GDNF* has been identified as a mesenchyme-derived signal that acts on the receptor tyrosine kinase (*Ret*) and *Gfrα1* coreceptor which are distributed in the ureteric epithelium and induces it to produce a ureteric bud which invades the metanephric mesenchyme (Sainio et al., 1997). Indeed, the null mutants of *GDNF*, *Ret* and *Gfrα1* show a similar perturbation of ureteric bud outgrowth (Schuchardt et al., 1994; Moore et al., 1996; Pichel et al., 1996; Sanchez et al., 1996; Cacalano et al., 1998). The homeodomain transcriptional factor *Six1* is expressed in the metanephric mesenchyme before and after induction, and *Six1*-knockout mice lack kidneys because of a failure of metanephric induction (Xu et al., 2003).

Sall1 is also expressed in the metanephric mesenchyme prior to bud invasion and continues in the induced condensing mesenchyme around ureteric bud tips and cells of mesenchymal origin. *Sall1* is the mouse homologue of *Drosophila sal* that is the region-specific homeotic gene characterized by unique multiple double zinc finger motifs (Kuhnlein et al., 1994). Humans and mice have at least four *sal*-related genes, respectively (*SALL1*, *-2*, *-3* and *-4* for humans and *Sall1*, *-2*, *-3* and *-4* for mice) (Kohlhase et al., 1996, 1999, 2000, 2002). *SALL1* is located on chromosome 16q12.1, and heterozygous mutations of *SALL1* lead to Townes-Brocks syndrome, an autosomal-dominant disease with features of dysplastic ears, preaxial polydactyly, imperforate anus and, less commonly, kidney and heart anomalies (Kohlhase et al., 1998). Mice deficient in *Sall1* die in the perinatal period, and kidney agenesis or severe dysgenesis are present (Nishinakamura et al., 2001). Homozygous deletion of *Sall1* results in an incomplete ureteric bud outgrowth and failure of tubule formation in the mesenchyme. Therefore, *Sall1* is essential for ureteric bud invasion, the initial key step in metanephros development.

At present only about 20 genes are known to have important roles for kidney development and the genetic cascade of kidney development is still largely unknown. Therefore there may exist unknown mesenchymal genes that are essential for kidney development and an efficient screening assay such as microarray analysis is needed to identify these genes. We did a microarray analysis with mesenchymal cells of *Sall1-GFP* knockin mice isolated by fluorescein-activated cell sorting (FACS). In this report we show that the combination of microarray analysis and *Sall1-GFP* knockin mice, is useful for identifying many mesenchymal genes.

2. Results

2.1. Generation of Sall1-GFP knockin mice

To label *Sall1*-expressing cells, green fluorescence protein (*GFP*) was knocked in the *Sall1* locus by homologous recombination. *GFP* was inserted into the *Eco*RI site of exon 2 so that N-terminal 52 amino acids of *Sall1* were fused in frame to *GFP* (Fig. 1A). Mice were genotyped using Southern blots (data not shown). This strategy is essentially the same as those used for *Sall1*-del and *Sall1-LacZ* mice that we reported, and all homozygous mice showed kidney agenesis or severe dysgenesis (data not shown). In contrast, heterozygous mice were phenotypically normal and were used for this study.

2.2. Expression pattern of GFP fluorescence in Sall1-GFP knockin kidneys

Prominent fluorescence of *GFP* was visible through the surface of brains, kidneys and limb buds of embryonic *Sall1-GFP* heterozygous mice. Microscopic analysis of the frozen section confirmed specific expression of *GFP* in cells of mesenchymal origin. Green fluorescence was observed throughout the metanephric mesenchyme, ranging from condensed mesenchyme, S-shaped bodies, to renal tubules (Fig. 1B). This expression pattern is consistent with *LacZ* expression of *Sall1-LacZ* knockin mice generated earlier (Fig. 1C) (Nishinakamura et al., 2001). *Sall1* expression was also observed in glomeruli in *Sall1-LacZ* mice, but not in *Sall1-GFP* mice perhaps due to the low sensitivity of *GFP*. Examination of both strains revealed *Sall1* expression in stromal cells, the outer most layer of the kidney, that was not noted in our earlier study.

2.3. Isolation of GFP-expressing kidney mesenchymal cells by FACS

To isolate *GFP*-positive cells from embryonic kidneys of these *Sall1-GFP* heterozygous mice, FACS analysis was used. Embryonic kidneys (17.5 dpc) were digested with collagenase, dissociated into single cells by pipetting and sorted. *GFP*-positive cells (12% of total kidney cells) and *GFP*-negative cells (20%) were isolated (Fig. 2A), and their purity was determined by reanalysis (94% of isolated *GFP*-positive cells and 99% of isolated *GFP*-negative cells were redetected in each gate).

Gene expression of each population was examined using RT-PCR (Fig. 2B). Indeed the positive population preferentially expressed *Sall1*, *GDNF* and *WT-1*, marker genes of mesenchymal cells, while the negative population

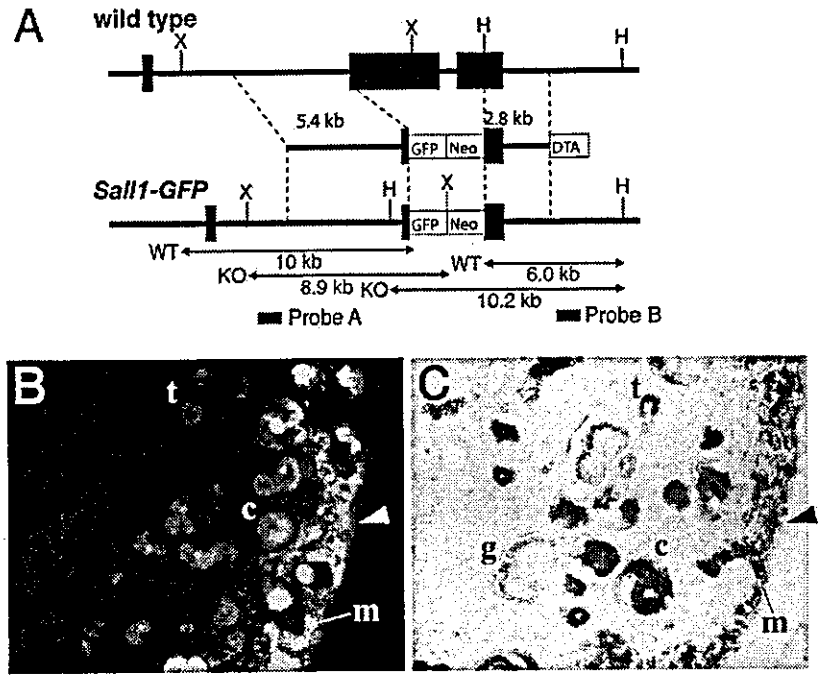

Fig. 1. Generation of *Sall1-GFP* knockin mice. (A) Targeting strategy of *Sall1-GFP* mice. *GFP* was knocked in the *Sall1* locus so that N-terminal 52 amino acids of *Sall1* was fused in frame to *GFP*. (B) *GFP* expression in embryonic kidney of heterozygous *Sall1-GFP* knockin mice. (C) X-gal staining of embryonic kidney in heterozygous *Sall1-LacZ* knockin mice. Arrowhead, stroma; m, condensed mesenchyme; c, comma-shaped bodies; t, tubles; g, glomerulus.

preferentially expressed *Ret*, a marker gene of the ureteric bud. A weak *Sall1* signal in the GFP-negative cells indicated that cells weakly expressing *Sall1* were included in the GFP-negative gate we defined in FACS analysis.

2.4. Demonstration of differential gene expression

To identify genes that are differentially expressed between *GFP*-positive and -negative populations, microarray analysis with Affymetrix GeneChip probe array was done. One microgram total RNA of each population isolated from the FACS analysis were individually amplified to 50 μg of cRNA by T7-mediated in vitro transcription, and each cRNA product was used to interrogate Mu74 GeneChips containing probe sets representing over 36,000 mouse genes and EST clusters. We identified 392 mRNAs expressed threefold greater in the *GFP*-positive population and sorted the list by the sort score determined using GeneChip software. The sort score is a ranking on the fold change and the absolute expression intensity. The higher the fold change and the absolute expression intensity become, the higher was the sort score. For example a gene whose absolute expression intensity changes from 100 in *GFP*-negative cells to 1000 in *GFP*-positive cells has a higher sort score than a gene whose absolute expression intensity changes from 1 to 10. Thus we obtained a statistical evaluation of differences in expression level of a gene based on the fold change and the absolute expression intensity.

We identified a large number of genes reported to be abundantly expressed in the metanephric mesenchyme, including *Sall1* (14-fold), *Glial cell line-derived neurotrophic factor* (*GDNF*) (39-fold), *Reelin* (14-fold), *Six-2* (9-fold), *Pax-8* (31-fold), *LRP-2* (7-fold), *PDGFc* (11-fold), *HeyL* (8-fold), *Cited-1* (8-fold), *Syndecan-4* (17-fold), *BMPR-1A* (8-fold) *WT-1* (7-fold), *FGF-10* (3-fold) and *BMP-7* (3-fold). We also detected stromal genes such as *Raldh-2* (23-fold) and *Fox D1* (6-fold), which is consistent with *Sall1* expression in this cell population. See supplementary

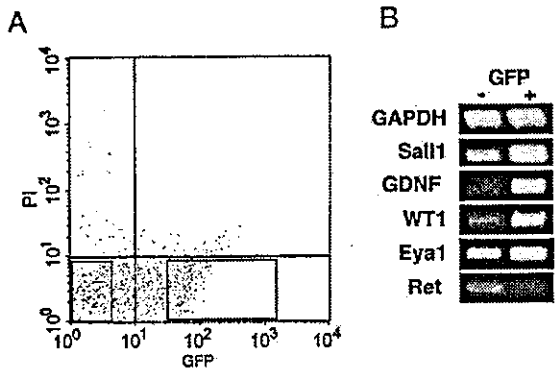

Fig. 2. FACS analysis of *Sall1-GFP* knockin embryonic kidney. (A) The distribution graph of dissociated kidney cells. We sorted *GFP*-positive (right square) and -negative population (left square). (B) RT-PCR analysis between *GFP*-positive (+) and -negative (−) population.

Table 1
Top 50 cDNAs detected abundantly in mesenchymal cells by microarray analysis

GenBank	Description	Mean (Sall1 −)	Mean (Sall1 +)	Fold change	Sort score	Test	Method
AA386439	Sall1	105.3	1531	14.2	14.68	+	Reported
D49921	GDNF	10.1	471.4	38.6	12.68	+	Reported
AJ001116	Unc4.1 homeobox	9.1	371.7	37.9	11.85	+	Reported
AW060720	Hormonally upregulated Neu-associated kinase	22.8	518	22.8	11.5	+	Reported
X99273	Raldh2	−13.7	226.1	42.5	10.16	+	Reported
AI844853	Gcnt2	−9.9	264.3	39.4	9.5	−	In situ
U24703	Reelin	42.3	577.1	14	9.12	+	Reported
AV302770	ESTs	58.1	540.3	11.8	8.69	+	In situ
AW213683	RIKEN cDNA 5730456K23 gene	10.7	445.9	18	8.06	+	In situ
D13903	Protein tyrosine phosphatase, receptor type, D	−0.9	172.3	32	7.86	+	Reported
X80338	Six2	98	880.2	9	7.79	+	Reported
AI152741	Odd-skipped related 2	−110.8	409.3	19.3	7.75	+	Reported
X57487	Paired box gene 8	0.7	161.1	31.1	7.66	+	Reported
AF030433	Dickkopf homolog 1	0	137.9	26.1	6.42	+	Reported
AI042846	LRP2	148.8	1015.3	6.9	6.38	+	Reported
AI842820	RIKEN cDNA 5730456K23 gene	49.1	485	9.9	6.29	+	In situ
M32352	Renin 2	623.6	2703.4	4.6	6.15	+	Reported
M83985	Snap91	5.4	164.5	24.4	6.06	−	In situ
AW045500	ESTs	6.7	252.5	10.2	5.82	+	In situ
AA929443	Amnionless	−35.1	223.3	13.7	5.67	−	In situ
AI851805	PDGFc	33.3	368.3	10.5	5.64	+	Reported
AV319451	Renin 1 structural	21.7	266.4	12.3	5.55	+	Reported
AI790931	Fbp1	50.2	467	8.9	5.46	+	In situ
U52842	Slc22a6	−4.1	114.5	22.2	5.4	+	In situ
X17320	Purkinje cell protein 4	1.2	111.5	22	5.36	+	Reported
AI854068	RIKEN cDNA 1110018M03 gene	81.8	567	7.4	5.33	−	In situ
AI462128	ESTs (A430091O)	90.5	649.3	7.2	5.33	+	In situ
AW208410	ESTs	36.9	377.1	9.4	5.28	−	In situ
AI314694	Nx17-pending	160.4	982.7	6	5.24	+	In situ
AI891653	ESTs	57.7	418.4	9.3	5.17	−	In situ
AI428510	RIKEN cDNA 2810004A10 gene	82.7	536	7.1	5	+	In situ
AI316329	Claudin 6	−219.9	94.7	17.8	4.75	+	In situ
AI854431	RIKEN cDNA 1110031N17 gene	135.4	793.8	5.9	4.66	−	In situ
AI604913	HeyL	44.3	365.3	8.3	4.61	+	Reported
L09192	Pyruvate decarboxylase	58.8	873	5.9	4.58	+	Reported
AI430929	Wnk4	262.3	1267.2	4.8	4.56	+	In situ
AI480529	RIKEN cDNA 6720429C22 gene	261.6	1257.4	4.8	4.51	+	In situ
X15789	Crabp1	0.4	95.6	18	4.32	+	Reported
J05663	Aldo–keto reductase family 1, member B7	64.4	321.2	7.7	4.2	+	Reported
U65091	Cited1	48.6	415.5	7.5	4.2	+	Reported
AI854068	RIKEN cDNA 1110018M03 gene	12.8	192.2	10.6	4.2	−	In situ
AA738774	Expressed sequence R75022	94.8	435.6	6.8	4.11	+	In situ
AI427519	Claudin 12	328.2	1417.6	4.3	4.09	−	In situ
AI326813	ESTs	−2.5	172.2	10.3	3.92	−	In situ
AF039391	μ-crystallin	9.8	124.4	12.7	3.87	+	In situ
AI837101	Calsyntenin 1	72.8	278.2	7.8	3.82	−	In situ
M21828	Gas2	37.8	287.8	7.6	3.77	+	In situ
D89571	Syndecan 4	−24.2	67.1	17.3	3.76	+	Reported
AA790312	ALCAM	399.9	1571.8	3.9	3.71	+	In situ
X63190	Etv4	1.8	81.3	15.2	3.56	+	In situ

Mean: expression intensity of cDNA. Test: (+) indicates that the cDNA proved to be a mesenchymal gene. (−) indicates that the cDNAs were proven to be negative. Method: Some cDNA were already noted in mesenchymal genes (Reported), and others were identified by mRNA in situ hybridization (in situ).

information for the complete data set (Supplementary information 1).

We also examined genes expressed more in *GFP*-negative cells than in the positive cells. We detected 612 mRNAs expressed threefold weaker in the *GFP*-positive cells (data not shown). We detected genes which are known to specifically expressed ureteric buds, such as *Wnt-11* (11-fold) and *TGFβ-1* (18-fold). However, many genes expressed in blood vessels were detected in these mRNAs which means that *GFP*-negative cells include not only ureteric buds but also cells derived from blood vessels.

To verify the result of microarray analysis, we subsequently did in situ hybridization for the top 50, except genes the expression patterns of which were previously

Table 2
Expression patterns of newly identified mesenchymal genes using microarray analysis

GenBank	Genes	Stromal cells	Condensed mesenchyme	S-, C-shaped bodies	Distal, proximal tubules	Glomeruli	Ureter
AI844853	Gcnt2	−	±	+	−	−	±
AV302770	ESTs	−	+	+	+	?	±
AW213683	5730456K23Rik	−	+	+	+	−	+
M83985	Snap91	−	−	±	−	−	−
AW045500	ESTs	−	+	−	−	−	−
AA929443	Amnionless	−	−	−	+	−	−
AI790931	Fbp1	−	+	+	+	+	−
U52842	Slc22a6	−	+	+	+	−	+
AI854068	1110018M03Rik	−	±	−	−	−	−
AI462128	ESTs (A430091O)	−	−	+	−	−	−
AW208410	ESTs	−	−	−	−	−	−
AI314694	Nx17-pending	−	+	+	+	?	+
AI891653	ESTs	−	−	−	−	−	−
AI428510	2810004A10Rik	−	+	+	−	−	−
AI316329	Claudin 6	−	−	−	−	−	+
AI854431	1110031N17Rik	−	−	−	−	−	−
AI430929	Wnk4	−	±	±	−	−	−
AI480529	6720429C22Rik	−	+	+	+	−	+
AA738774	R75022	−	+	+	+	−	−
AI427519	Claudin-12	−	−	−	−	−	±
AI326813	ESTs	−	−	−	−	−	−
AF039391	μ-crystallin	−	+	−	−	−	−
AI837101	Calsyntenin 1	−	−	−	−	−	−
M21828	Gas2	−	−	+	−	−	±
AA790312	ALCAM	+	−	−	−	−	−
X63190	Etv4	−	+	+	+	−	+
AI838599	ESTs	−	−	−	−	−	−
AI837711	ESTs(AK049098)	+	−	−	−	−	−
AI843433	ESTs(AW049604)	−	−	−	−	−	−
AI851210	ESTs(AK081204)	−	−	−	−	−	−
AI315647	Cors26	−	−	−	−	−	−
AW120700	ESTs(AW120700)	−	+	±	±	+	±
AI891500	1700011H14Rik	−	−	−	−	−	+
AI503543	SSB-4	−	±	+	−	−	+
AI838112	Smarcd3	−	+	−	−	−	+
AI152966	FLJ22569	−	+	−	−	−	±
AA727914	ESTs(AV158822)	−	−	−	−	−	+
AI836553	1110038H03Rik	−	±	+	−	−	−
AV071536	ESTs	−	−	−	−	−	±
AI463306	AW555464	−	+	+	−	−	−
AU021802	ESTs	−	−	−	−	−	−
AV336991	ESTs	−	−	−	−	−	−
AW124490	3000002J10Rik	−	±	−	−	−	−
AW050290	2810406K24Rik	−	+	−	−	−	−
AI842510	TRB-2	−	−	−	−	+	−

The expression pattern of each cDNAs was classified based on compartments of the kidney. The cDNAs were listed in order of sort score. The expression levels are represented by: (+) abundantly, (−) not detected, (±) weakly, (?) unknown.

reported (Table 1). The expression patterns of most of the genes were in good correlation with the results of our microarray analysis. 78% of the top 50 was confirmed to be expressed in the condensed mesenchyme, stromal cells, metanephric tubles or glomeruli. Out of top 50 mRNAs, 22 were previously reported as mesenchymal genes, 17 are newly identified ones as mesenchymal genes in the present work and 11 are not expressed in the mesenchyme. This indicates that most of the genes detected in the *GFP*-positive population using microarray analysis are indeed expressed abundantly in cells of mesenchymal origin or stromal cells.

2.5. Expression pattern of novel mesenchymal genes in the developing kidney

To determine which cells of the developing kidney express mesenchymal genes detected by microarray analysis, in situ hybridization with selected mRNAs was

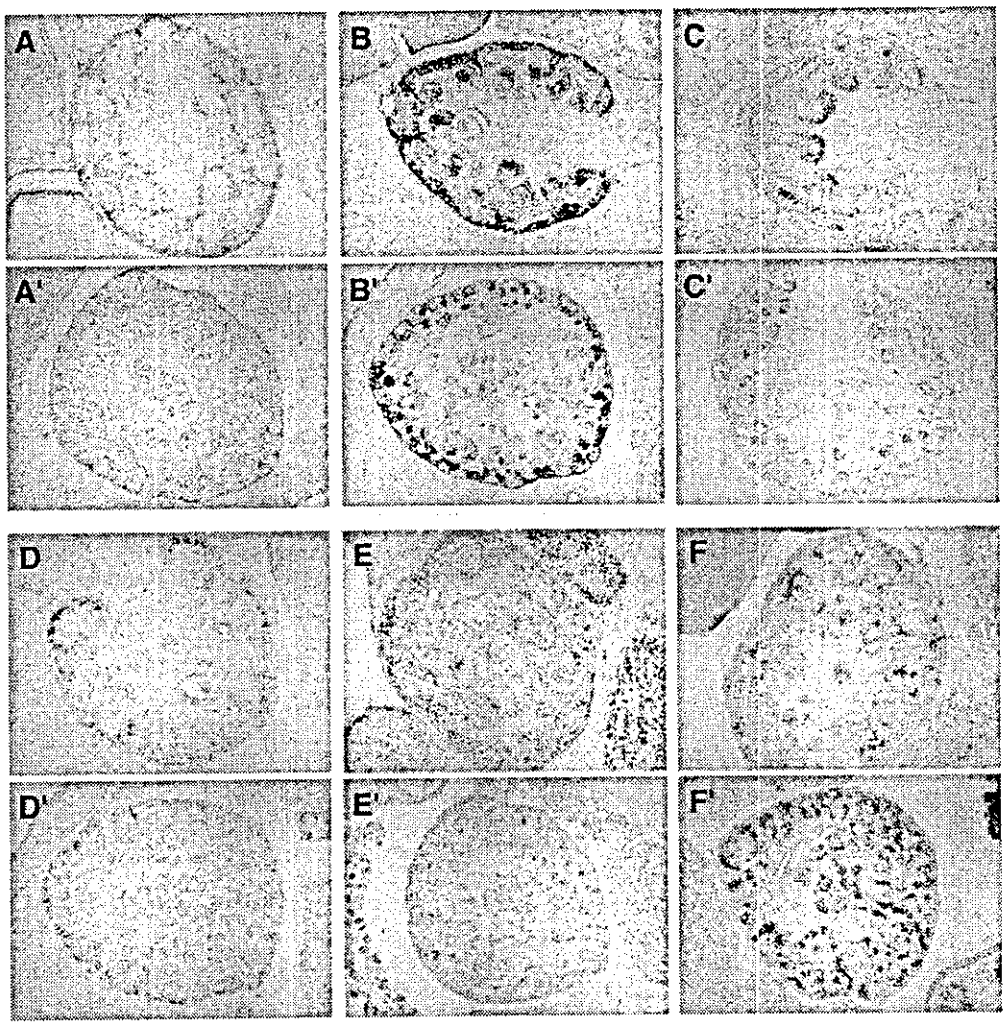

Fig. 3. In situ hybridization of fetal kidney. Upper panels are sections of 14.5 dpc and lower panels are those of 17.5 dpc. (A), (A′) *ALCAM*. (B), (B′) *Raldh2*. (C), (C′) *TRB-2*. (D), (D′) *μ-crystallin*. (E), (E′) *Smarcd3*. (F), (F′) *SSB-4*.

done (Table 2). We examined the top 50 mRNAs as well as mRNAs which gave high 'fold change' or high 'absolute expression intensity' in GFP-positive cells. We found that many genes defined as mesenchymal by microarray analysis were indeed expressed in the metanephric mesenchyme, including *ALCAM, SSB-4, Smarcd3, μ-crystallin, TRB-2*. These genes have not been previously reported as mesenchymal genes. In situ hybridization of these genes at two stages is shown in Fig. 3 (Supplementary information 2 for detailed images). 14.5 dpc is the stage representing development of the nephron in process, and 17.5 dpc is the stage at which RNA samples were collected.

ALCAM was first identified on thymic epithelial cells (Patel et al., 1995). *ALCAM* is a member of the Ig superfamily containing five extracellular Ig domains, and it activates leukocytes (Bowen et al., 1995). Arai et al. reported that *ALCAM*-positive perichondrial cells can differentiate into multiple lineages and the addition of *ALCAM*-Fc to metatarsal cultures inhibits the invasion of the blood vessels to a cartilage (Arai et al., 2002). We found that *ALCAM* was expressed abundantly in stromal cells, consisting with *Sall1* expression in the stromal region (Fig. 3A,A′).

The *Raldh2* gene codes for a retinaldehyde dehydrogenase that catalyzes the second oxidative step in the biosynthesis of retinoic acid (RA) from retinol (Zhao et al., 1996). *Raldh2* is responsible for most of the RA-synthesizing activity during early mouse embryogenesis (7.5–9.5 dpc), as seen from the failure of *Raldh2* − /− embryos to activate RA-responsive transgenes (Niederreither et al., 1999). These mutant embryos, which die at E9.5–10.5 from severe cardiac defects, exhibit axial truncation due to impaired somite growth, as well as hindbrain defects

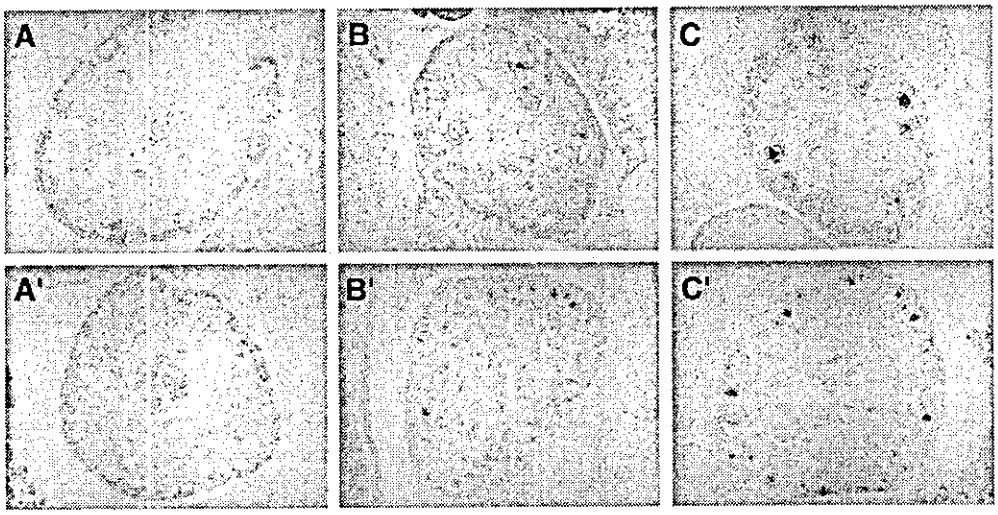

Fig. 4. In situ hybridization of ESTs in the fetal kidney. Upper panels are sections of 14.5 dpc and lower panels are those of 17.5 dpc. (A), (A′) BC023483. (B), (B′) 2810004A10Rik. (C), (C′) 1110038H03Rik.

(Niederreither et al., 1999, 2000, 2001). Our in situ hybridization showed *Raldh2* to be expressed in the stromal region (Fig. 3B,B′). Identification of two stromal genes (*ALCAM* and *Raldh2*) further proves that *Sall1* is also expressed in the stromal region.

TRB-2 is a mammalian homolog of *Drosophila tribbles*, which causes the degradation of *String/CDC25* and blocks mitosis. *TRB-2* was specifically expressed in the comma-, S-shaped bodies and glomeruli (Fig. 3C,C′). *TRB-3* was shown to be involved in insulin signaling (Du et al., 2003), which was the first demonstration that this family is important in mammals.

μ-crystallin is one of the taxon-specific crystallins and the predicted amino acid sequence indicates that *μ-crystallin* might have an enzymatic rather than a structural role in lens tissue (Kim et al., 1992; Vie et al., 1997). We specifically detected *μ-crystallin* in the condensed mesenchyme of the metanephric kidney (Fig. 3D,D′).

Smarcd3 is the member of the SWI/SNF family, the members of which display helicase and ATPase activities and which are thought to regulate transcription of certain genes by altering the chromatin structure around those genes (Ring et al., 1998). The encoded protein is part of the large ATP-dependent chromatin remodeling complex SNF/SWI. Our in situ hybridization showed *Smarcd3* to be abundantly expressed in the condensed mesenchyme, S-, comma-shaped bodies and weakly in the ureteric buds and collecting ducts (Fig. 3E,E′).

SSB-4 is a member of family of proteins that contain a C-terminal SOCS box and a SPRY domain. *SSB-4* was expressed abundantly in the condensed mesenchyme, glomerulus and weakly in ureteric buds and collecting ducts (Fig. 3F,F′).

We also examined expression patterns of some ESTs (Fig. 4). BC023483 was specifically expressed in the condensed mesenchyme (Fig. 4A). 2810004A10Rik was expressed abundantly in the S-, comma-shaped bodies and weakly in the condensed mesenchyme (Fig. 4B). 1110038H03Rik was expressed abundantly in S-, comma-shaped bodies and weakly in the condensed mesenchyme (Fig. 4C).

Taken together, it is evident that a combination of microarray analysis and *Sall1-GFP* knockin mice is useful for identification of kidney mesenchymal genes.

2.6. Mesenchymal genes in Sall1 knockout mice

This analysis also means that detected genes should colocalize with *Sall1* at various stages of metanephric development. The genes detected using our microarray analysis possibly include genes interacting with *Sall1*, genes downstream or upstream of *Sall1*, and these candidate genes could be essential for metanephric development. Colocalization of candidate genes with *Sall1* allows one to hypothesize that those genes could be regulated by critical transcription factors for kidney development, including *Sall1*. To clarify whether detected genes are downstream targets of *Sall1*, in situ hybridization in the developing kidney of *Sall1* knockout mice was done (11.5 dpc). At 11.5 dpc, uninduced condensed mesenchyme exists in *Sall1* knockout mice, but is reduced in size. We found 10 genes in the top 50 that were expressed in the condensed mesenchyme at 11.5 dpc. In *Sall1* knockout mice, expression levels of all the genes were either intact (*Six2, Raldh2, PDGFc, ALCAM, Hunk, Gas2, μ-crystallin*) or reduced (*Pax8, Unc4.1, GDNF*) (Fig. 5 and data not shown), and no gene was completely absent. Reduction in expression level of some genes could occur by metanephric mesenchymal reduction in size in *Sall1* knockout mice (Nishinakamura et al., 2001). In this case, transcription

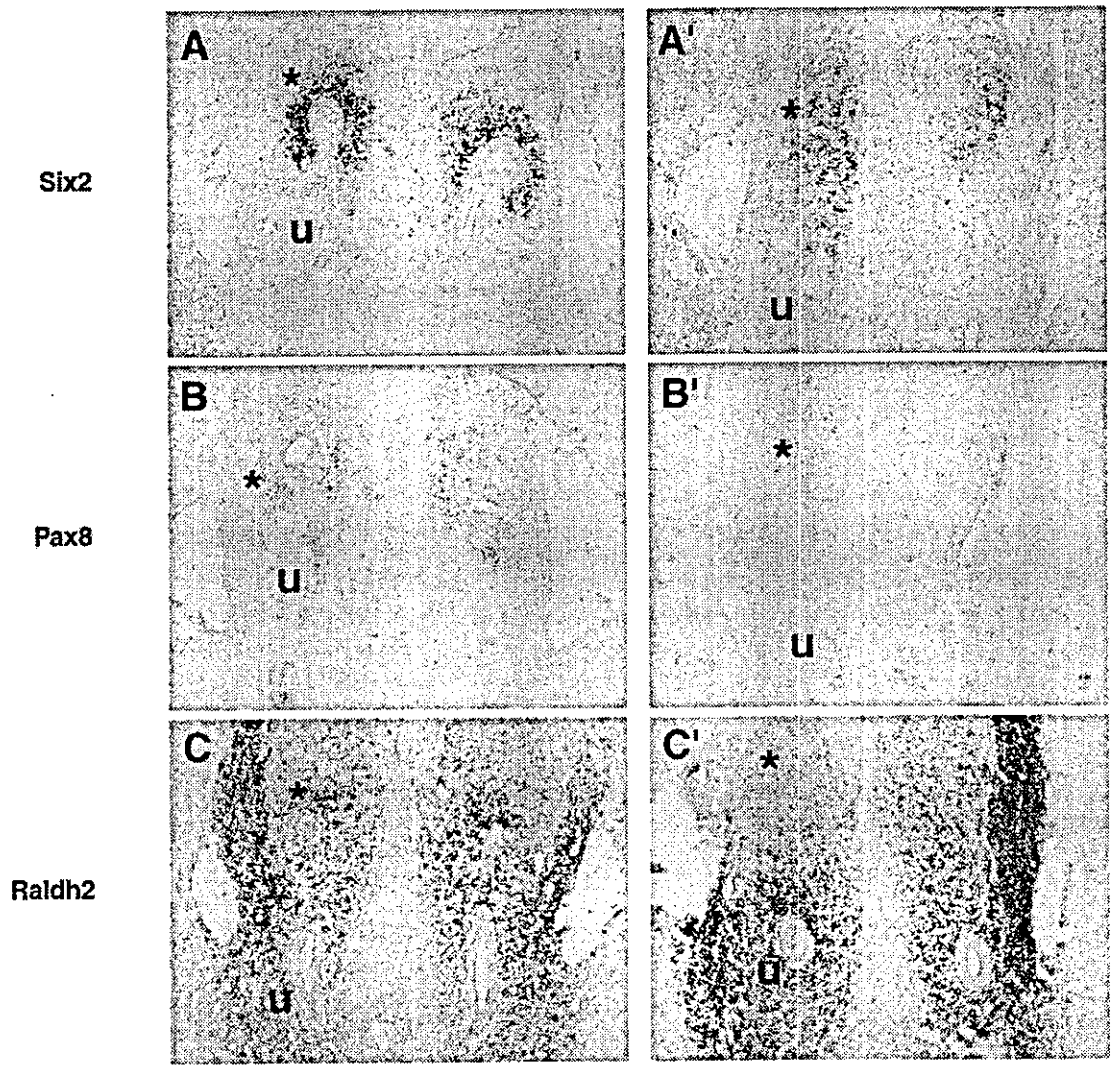

Fig. 5. In situ hybridization of mesenchymal genes in *Sall1* knockout (A′,B′,C′) and wild type mice (A,B,C) at 11.5 dpc. (A), (A′) *Six2*. (B), (B′) *Pax8*. (C), (C′) *Raldh2*. u, ureteric buds; asterisk (*), condensed mesenchyme.

factors other than *Sall1* could regulate the candidate genes, and utilization of mice lacking other critical transcription factors would be needed to clarify genetic cascades involved in candidate genes detected in this present work. Alternatively it could be possible that they are downstream targets of *Sall1* and loss of *Sall1* is compensated for by other transcription factors or *Sall* family genes (*Sall2*, *Sall3* and *Sall4*). To demonstrate this possibility, generating mice lacking both *Sall1* and another transcription factor or mice lacking all the *Sall* family genes is awaited.

3. Discussion

In the developing kidney, *Sall1* is expressed in the stroma region and cells of mesenchymal origin, including condensed mesenchyme, S-, comma-shaped bodies, podocytes, Bowman's capsule and distal, proximal tubles, while cells not expressing *Sall1* are collecting ducts, ureteric buds, medullary zone and blood vessels. This means that a comparison analysis of gene expression profiles in *Sall1*-positive and -negative cells can identify mesenchymal genes. Indeed we could detect many well-known mesenchymal genes using microarray analysis, including *GDNF*, *Raldh-2*, *Reelin*, *Six-2*, *Pax-8*, *LRP-2*, *PDGFc*, *HeyL*, *Cited-1*, *Syndecan-4*, *BMPR-1A*, *WT-1*, *FoxD1*, *FGF-10* and *BMP-7*. Our in situ hybridization analysis showed that 78% of the top 50 mRNAs of the microarray list were specifically expressed in cells of mesenchymal origin or the stroma. This supports the notion that many mesenchymal genes are enriched in *Sall1*-positive cells. Moreover we found unknown mesenchymal genes and ESTs that are expressed

in cells of mesenchymal origin, using in situ hybridization, including *μ-crystallin, ALCAM, SSB-4, Smarcd3* and *TRB-2*. Thus we demonstrate that a combination of microarray technology and *Sall1-GFP* knockin mice is useful for efficient identification of mesenchymal genes expressed in the developing kidney.

Though kidney development is indeed a complicated system, no more than 20 genes have been identified as being essential. In this report, we identified a large number of mesenchymal genes in the developing kidney. To find essential genes from this large list, efficient and rapid screening is needed. Recently emerging siRNA technology is one potent method. Indeed Sakai et al. reported that transfection of siRNA into the metanephros followed by organ culture was useful for demonstrating essential roles of fibronectin in the developing kidney (Sakai et al., 2003). A similar approach could be used for our candidate genes. However, interpretation can be risky. A variety of genes was reported to be essential for kidney development, using conventional antisense oligo nucleotides and organ culture technology, but many proved negative when subjected to gene targeting. Therefore generating knockout mice of each candidate gene is necessary for proof. Establishment of a kidney-specific knockout system could also be useful for the purpose.

We showed that *Sall1, GDNF*, and *Raldh-2*, the genes essential for metanephric development, rank high in our gene chip list. *GDNF* is expressed in the metanephric mesenchyme before ureteric bud initiation. Null mutation of *GDNF* has severe kidney phenotypes, ranging from no ureteric bud formation to rudimentary kidney formation, which is very close to the phenotype of *Sall1* mutant mice. Retinaldehyde dehydrogenase-2 (*Raldh2*) is required for most embryonic RA synthesis (Niederreither et al., 1999) and is expressed in stromal cells (Fig. 3F,F′). *Raldh2, RARα* and *RARβ2* are colocalized in the cortical stroma, and knockout mouse studies showed that RA is important in the cortical stroma for generating signals that control branching morphogenesis by regulating *Ret* expression in the ureteric bud (Batourina et al., 2001). *Sall1* could be involved in these *GDNF-Ret* and/or RA-*Ret* pathways, though *Raldh2* is unlikely to be a downstream target of *Sall1*, as shown by intact *Raldh2* expression in *Sall1* knockout mice (Fig. 5C).

In conclusion, we identified many mesenchymal genes, and demonstrated that using a combination of microarray technology and *Sall1-GFP* knockin mouse is a pertinent means of identifying mesenchymal genes systematically. A similar approach may be applicable to other organs, such as brains and limb buds where *Sall1* is expressed.

4. Experimental procedures

4.1. Generation of GFP knockin mice

A Sal-NotI *GFP* fragment (769 bp) from pEGFP-N1 (Clontech) was fused to the *Sal*I-*Pac*I site of pxCAN-LacZ (RIKEN), then the 5′ *Sma*I-*Sma*I 5.4 kb fragment was fused to the *Bam*HI site of this vector in frame. Finally, the resultant *Sal*I-*Xho*I 6.7 kb fragment was cloned into the *Xho*I site of the vector, that contained the neomycin-resistant (neo^r) gene (pMC1-neo polyA), 3′ *Hin*dIII-*Cla*I 2.8 kb fragment and a diphtheria toxin A subunit (pMC1-DTA) in tandem.

E14.1 embryonic stem cells were plated on mitomycin C-treated primary embryonic fibroblasts, and clones resistant to G418 (400 μg/ml) were screened using Southern blots. The genomic DNA from clones was digested with *Hin*dIII, electrophoresed through 0.7% agarose, transferred to nylon membrane (HybondN +, Amersham-Pharmacia), and hybridized to a radioactive probe. The probe used to screen the samples was a *Cla*I-*Eco*RI 1.2 kb fragment downstream of 3′ homology (probe B). The samples were also digested with *Xho*I, and hybridized with a 5′ probe (probe A) to confirm the correct homologous recombination. A probe corresponding to the Neo sequence was also used to verify that only one copy of the vector was integrated into the genome. Of 120 clones, six were correctly targeted for *Sall1-GFP*.

Recipient blastocysts were from C57BL/6J mice. Chimeric animals were bred with C57BL/6J females. Mutant animals studied were of F_2 and F_3 generations. Mice were genotyped using Southern blots or genomic PCR. The primer sequences used for PCR were as follows: AGCTAAAGCTGCCAGAGTGC, CAACTTGCGATT GCCATAAA, and GCGTTGGCTACCCGTGATAT (288 bp for the wild-type Sall1 allele, and 350 bp for the mutated allele).

4.2. Fluorescein-activated cell sorting

Cell suspension was prepared from kidney of *Sall1-GFP* knockin mice (17.5 dpc). Kidneys were digested with 0.25% collagenase type B (Roche Diagnostics) at 37 °C for 1 h, and cells were dissociated using fine-tipped pipettes. After the cells had been filtered through a 35 μm nylon mesh, they were resuspended in PBS containing 0.5% FCS and 1 mM EDTA at a final concentration of 2×10^6 cells/ml. Propidium Iodide (Sigma-Aldrich) was added at a final concentration of 50 μg/ml to label the dead cells.

FACS analysis was done with the FACS Vantage (Becton Dickinson Immunocytometry Systems). Dead cells were excluded from the plots based on propidium iodide. The isolated cells were centrifuged at 1000 rpm for 5 min and resuspended in TRIzol Reagent (Invitrogen).

4.3. RNA amplification for array analysis

MessageAmp™ aRNA Kits (Ambion) were used according to the manufacturer's instructions. Briefly, 11 μl of 1 μg total RNA and 1 μl of T7-Oligo(dT) Primer incubated at 70 °C for 10 min, was followed by incubation at 42 °C for 5 min. Next, 2 μl of 10× First Strand Buffer, 1 μl of Ribonuclease Inhibitor and 4 μl of dNTP Mix were added,

and incubation continued at 42 °C for 2 h. Next, 63 μl of RNase-free H_2O, 10 μl of 10 × Second Strand Buffer, 4 μl of dNTP Mix, 2 μl of DNA Polymerase and 1 μl of RNase H, and the mixture was incubated at 16 °C for 2 h. Next, the cDNA was purified, and dried down to 8 μl for in vitro transcription. For in vitro transcription, 8 μl of the purified cDNA, dried biotin-CTP and -UTP, 2 μl of T7 ATP Solution (75 mM), 1.5 μl of T7 CTP Solution (75 mM), 2 μl of T7 GTP Solution (75 mM), 1.5 μl of T7 UTP Solution (75 mM), 2 μl of Enzyme Mix, and 1 μl of RNase-free H_2O were incubated at 37 °C for 12 h. Then 2 μl of DNase 1 was added and incubated at 37 °C for 30 min, followed by antisense RNA purification.

4.4. Microarray analysis

The Affymetrix Murine Genome U74v2 Set was used to compare gene expression profiles of the GFP-positive and -negative cells according to manufacturer's protocols. Briefly, biotinylated cRNAs were synthesized and hybridized to the GeneChip probe arrays, which were then washed in washing solution, stained with streptavidin–phycoerythrin and scanned. Analysis was made using Affymetrix GeneChip software. Two independent RNA samples were prepared and similar results were obtained using Mu74A GeneChip, then one of two samples was used for Mu74 complete GeneChip (Mu74A, B and C).

4.5. In situ hybridization

In situ hybridization was done using digoxigenin-labeled antisense riboprobes as described (Nishinakamura et al., 2001). Fragments were amplified using PCR, subcloned into pCRII (Invitrogen), and sequenced. None of the sense probes yielded signals.

Acknowledgements

We thank Miyuki Itoh for technical assistance. The Division of Stem Cell Regulation is supported by Amgen Limited. The work was partly supported by grants from Research for the Future Program in Ministry of Education, Science, Technology, Sports and Culture, Japan.

References

Arai, F., Ohneda, O., Miyamoto, T., Zhang, X.Q., Suda, T., 2002. Mesenchymal stem cells in perichondrium express activated leukocyte cell adhesion molecule and participate in bone marrow formation. J. Exp. Med. 195, 1549–1563.

Batourina, E., Gim, S., Bello, N., Shy, M., Clagett-Dame, M., Srinivas, S., et al., 2001. Vitamin A controls epithelial/mesenchymal interactions through Ret expression. Nat. Genet. 27, 74–78.

Bowen, M.A., Patel, D.D., Li, X., Modrell, B., Malacko, A.R., Wang, W.C., et al., 1995. Cloning, mapping, and characterization of activated leukocyte-cell adhesion molecule (ALCAM), a CD6 ligand. J. Exp. Med. 181, 2213–2220.

Buller, C., Xu, X., Marquis, V., Schwanke, R., Xu, P.X., 2001. Molecular effects of Eya1 domain mutations causing organ defects in BOR syndrome. Hum. Mol. Genet. 10, 2775–2781.

Cacalano, G., Farinas, I., Wang, L.C., Hagler, K., Forgie, A., Moore, M., et al., 1998. GFRalpha1 is an essential receptor component for GDNF in the developing nervous system and kidney. Neuron 21, 53–62.

Du, K., Herzig, S., Kulkarni, R.N., Montminy, M., 2003. TRB3: a tribbles homolog that inhibits Akt/PKB activation by insulin in liver. Science 300, 1574–1577.

Herzlinger, D., Koseki, C., Mikawa, T., al-Awqati, Q., 1992. Metanephric mesenchyme contains multipotent stem cells whose fate is restricted after induction. Development 114, 565–572.

Kim, R.Y., Gasser, R., Wistow, G.J., 1992. mu-crystallin is a mammalian homologue of Agrobacterium ornithine cyclodeaminase and is expressed in human retina. Proc. Natl Acad. Sci. USA 89, 9292–9296.

Kohlhase, J., Schuh, R., Dowe, G., Kuhnlein, R.P., Jackle, H., Schroeder, B., et al., 1996. Isolation, characterization, and organ-specific expression of two novel human zinc finger genes related to the Drosophila gene spalt. Genomics 38, 291–298.

Kohlhase, J., Wischermann, A., Reichenbach, H., Froster, U., Engel, W., 1998. Mutations in the SALL1 putative transcription factor gene cause Townes-Brocks syndrome. Nat. Genet. 18, 81–83.

Kohlhase, J., Hausmann, S., Stojmenovic, G., Dixkens, C., Bink, K., Schulz-Schaeffer, W., et al., 1999. SALL3, a new member of the human spalt-like gene family, maps to 18q23. Genomics 62, 216–222.

Kohlhase, J., Altmann, M., Archangelo, L., Dixkens, C., Engel, W., 2000. Genomic cloning, chromosomal mapping, and expression analysis of msal-2. Mamm. Genome 11, 64–68.

Kohlhase, J., Heinrich, M., Schubert, L., Liebers, M., Kispert, A., Laccone, F., et al., 2002. Okihiro syndrome is caused by SALL4 mutations. Hum. Mol. Genet. 11, 2979–2987.

Kreidberg, J.A., Sariola, H., Loring, J.M., Maeda, M., Pelletier, J., Housman, D., et al., 1993. WT-1 is required for early kidney development. Cell 74, 679–691.

Kuhnlein, R.P., Frommer, G., Friedrich, M., Gonzalez-Gaitan, M., Weber, A., Wagner-Bernholz, J.F., et al., 1994. Spalt encodes an evolutionarily conserved zinc finger protein of novel structure which provides homeotic gene function in the head and tail region of the Drosophila embryo. Eur. Mol. Biol. Org. J. 13, 168–179.

Moore, M.W., Klein, R.D., Farinas, I., Sauer, H., Armanini, M., Phillips, H., et al., 1996. Renal and neuronal abnormalities in mice lacking GDNF. Nature 382, 76–79.

Niederreither, K., Subbarayan, V., Dolle, P., Chambon, P., 1999. Embryonic retinoic acid synthesis is essential for early mouse post-implantation development. Nat. Genet. 21, 444–448.

Niederreither, K., Vermot, J., Schuhbaur, B., Chambon, P., Dolle, P., 2000. Retinoic acid synthesis and hindbrain patterning in the mouse embryo. Development 127, 75–85.

Niederreither, K., Vermot, J., Messaddeq, N., Schuhbaur, B., Chambon, P., Dolle, P., 2001. Embryonic retinoic acid synthesis is essential for heart morphogenesis in the mouse. Development 128, 1019–1031.

Nishinakamura, R., Matsumoto, Y., Nakao, K., Nakamura, K., Sato, A., Copeland, N.G., et al., 2001. Murine homolog of SALL1 is essential for ureteric bud invasion in kidney development. Development 128, 3105–3115.

Patel, D.D., Wee, S.F., Whichard, L.P., Bowen, M.A., Pesando, J.M., Aruffo, A., et al., 1995. Identification and characterization of a 100-kD ligand for CD6 on human thymic epithelial cells. J. Exp. Med. 181, 1563–1568.

Pichel, J.G., Shen, L., Sheng, H.Z., Granholm, A.C., Drago, J., Grinberg, A., et al., 1996. Defects in enteric innervation and kidney development in mice lacking GDNF. Nature 382, 73–76.

Ring, H.Z., Vameghi-Meyers, V., Wang, W., Crabtree, G.R., Francke, U., 1998. Five SWI/SNF-related, matrix-associated, actin-dependent

regulator of chromatin (SMARC) genes are dispersed in the human genome. Genomics 51, 140–143.

Sainio, K., Suvanto, P., Davies, J., Wartiovaara, J., Wartiovaara, K., Saarma, M., et al., 1997. Glial-cell-line-derived neurotrophic factor is required for bud initiation from ureteric epithelium. Development 124, 4077–4087.

Sakai, T., Larsen, M., Yamada, K.M., 2003. Fibronectin requirement in branching morphogenesis. Nature 423, 876–881.

Sanchez, M.P., Silos-Santiago, I., Frisen, J., He, B., Lira, S.A., Barbacid, M., 1996. Renal agenesis and the absence of enteric neurons in mice lacking GDNF. Nature 382, 70–73.

Schuchardt, A., D'Agati, V., Larsson-Blomberg, L., Costantini, F., Pachnis, V., 1994. Defects in the kidney and enteric nervous system of mice lacking the tyrosine kinase receptor Ret. Nature 367, 380–383.

Vie, M.P., Evrard, C., Osty, J., Breton-Gilet, A., Blanchet, P., Pomerance, M., et al., 1997. Purification, molecular cloning, and functional expression of the human nicodinamide-adenine dinucleotide phosphate-regulated thyroid hormone-binding protein. Mol. Endocrinol. 11, 1728–1736.

Xu, P.X., Adams, J., Peters, H., Brown, M.C., Heaney, S., Maas, R., 1999. Eya1-deficient mice lack ears and kidneys and show abnormal apoptosis of organ primordia. Nat. Genet. 23, 113–117.

Xu, P.X., Zheng, W., Huang, L., Maire, P., Laclef, C., Silvius, D., 2003. Six1 is required for the early organogenesis of mammalian kidney. Development 130, 3085–3094.

Zhao, D., McCaffery, P., Ivins, K.J., Neve, R.L., Hogan, P., Chin, W.W., et al., 1996. Molecular identification of a major retinoic-acid-synthesizing enzyme, a retinaldehyde-specific dehydrogenase. Eur. J. Biochem. 240, 15–22.

A novel chordin-like BMP inhibitor, CHL2, expressed preferentially in chondrocytes of developing cartilage and osteoarthritic joint cartilage

Naoki Nakayama[1,*,†], Chun-ya E. Han[1], Linh Cam[2], Jae I. Lee[1], Jim Pretorius[3], Seth Fisher[4], Robert Rosenfeld[4], Sheila Scully[3], Ryuichi Nishinakamura[5], Diane Duryea[3], Gwyneth Van[3], Brad Bolon[3], Takashi Yokota[5] and Ke Zhang[2]

[1]Department of Metabolic Disorders, Amgen, One Amgen Center Drive, Thousand Oaks, CA 91320, USA
[2]Department of Cancer Biology, Amgen, One Amgen Center Drive, Thousand Oaks, CA 91320, USA
[3]Department of Pathology, Amgen, One Amgen Center Drive, Thousand Oaks, CA 91320, USA
[4]Department of Protein Science, Amgen, One Amgen Center Drive, Thousand Oaks, CA 91320, USA
[5]Department of Stem Cell Regulation, Institute of Medical Science, The University of Tokyo, 4-6-1 Shirokanedai, Minato-ku, Tokyo 108-8639, Japan
*Present address: National Stem Cell Centre in Stem Cell Biology Laboratory, Peter MacCallum Cancer Institute, St Andrews Place, East Melbourne, VIC 3002, Australia
†Author for correspondence (e-mail: naoki.nakayama@petermac.org)

Accepted 2 October 2003

Development 131, 229-240
Published by The Company of Biologists 2004
doi:10.1242/dev.00901

Summary

We have identified a novel chordin-like protein, CHL2, which is structurally most homologous to CHL/neuralin/ventroptin. When injected into *Xenopus* embryos, CHL2 RNA induced a secondary axis. Recombinant CHL2 protein interacted directly with BMPs in a competitive manner to prevent binding to the type I BMP receptor ectodomain, and inhibited BMP-dependent induction of alkaline phosphatase in C2C12 cells. Thus, CHL2 behaves as a secreted BMP-binding inhibitor. In situ hybridization revealed that *CHL2* expression is restricted to chondrocytes of various developing joint cartilage surfaces and connective tissues in reproductive organs. Adult mesenchymal progenitor cells expressed *CHL2*, and its levels decreased during chondrogenic differentiation. Addition of CHL2 protein to a chondrogenic culture system reduced cartilage matrix deposition. Consistently, CHL2 transcripts were weakly detected in normal adult joint cartilage. However, *CHL2* expression was upregulated in middle zone chondrocytes in osteoarthritic joint cartilage (where hypertrophic markers are induced). CHL2 depressed chondrocyte mineralization when added during the hypertrophic differentiation of cultured hyaline cartilage particles. Thus, CHL2 may play negative roles in the (re)generation and maturation of articular chondrocytes in the hyaline cartilage of both developing and degenerated joints.

Key words: Secreted protein, Chordin, BMP, Inhibitor, Chondrocyte, Cartilage, Superficial zone, Joint, Osteoarthritis

Introduction

Bone morphogenetic proteins (BMPs) belong to the transforming growth factor (TGF) β super family. These molecules play important roles during many organogenic processes, even though they were originally identified as factors promoting the ectopic formation of cartilage and bone. The concentration of active BMP is controlled in part by inhibitors from three BMP binding protein families: short gastrulation/chordin, noggin and cerberus (reviewed by Balemans and Van Hul, 2002). Among these, chordin and noggin were the first proteins found to inhibit the activity of bound BMPs by preventing interactions with their BMP receptors (Piccolo et al., 1996; Zimmerman et al., 1996). Although noggin is encoded by a single gene in mammals, chordin belongs to a family of proteins that share a cysteine-rich pro-collagen repeat [or chordin-like cysteine-rich repeat (CR)], which is also found in various extracellular matrix proteins (reviewed by Garcia Abreu et al., 2002). Without exception, the homology between chordin family members lies within their CRs.

The chordin polypeptide contains four CRs, of which the first and the third (CR1 and CR3) are responsible for BMP binding (Larrain et al., 2000). Binding of chordin to BMP4 is specific and tight (Piccolo et al., 1996). Proteolysis by Tolloid (or BMP1), which liberates CR1 and CR4 from chordin, is required to release bound BMP4 (Piccolo et al., 1997; Scott et al., 1999). The importance of CR for BMP interactions has been strengthened by the recent finding that connective tissue growth factor functions as a BMP-binding inhibitor, and that its single CR domain is essential for this activity (Abreu et al., 2002).

We previously described a small chordin-like secreted protein, CHL1 (for chordin-like 1, re-designated from CHL), a novel BMP-binding inhibitor with three CRs (Nakayama et al., 2001). CHL1 was isolated originally from mouse bone marrow stromal cells. Interestingly, *CHL1* expression

correlates with the stem/progenitor-support activities of over 19 stromal cell lines established from the aorta-gonads-mesonephros region, the site at which definitive hematopoietic stem cells first arise during embryogenesis (Oostendorp et al., 2002). However, CHL1 mRNA is also detected in various mesenchymal derivatives associated with (1) the dermatome, limb bud and chondrocyte precursors of the skeleton during embryogenesis, and (2) digestive tract connective tissues, kidney tubules and marrow stromal cells in adults. In addition, *CHL1* is expressed in olfactory bulb and cerebellum, suggesting a wider array of physiological functions. Two other groups have independently isolated CHL1, naming it neuralin-1 and ventroptin (Coffinier et al., 2001; Sakuta et al., 2001) and demonstrating its ability to correctly specify retinotectal projections along the dorsoventral retinal axis during development.

We provide evidence that CHL2, a novel chordin family member with structural homology to CHL1, is a BMP-binding inhibitor whose expression is uniquely restricted to the superficial layers of developing joint cartilage, in contrast to that of other family members. Potential downregulation of cartilage matrix accumulation and/or cartilage mineralization by CHL2 is suggested by in vitro observations using cartilage particles derived from embryonic stem (ES), cell-derived mesodermal cells (Nakayama et al., 2003) and with marrow-derived mesenchymal stem/progenitor cells (MSCs). CHL2 is also induced in osteoarthritic joint cartilage, implying a potential role during cartilage regeneration in the adult.

Materials and methods

Cells and reagents

Enzymes for the polymerase chain reaction (PCR) and cDNA library constructions; recombinant human proteins (and corresponding antibodies for western blot detection) for BMP4, BMP5, BMP6, activin A, TGFβ2, and BMP receptor 1B-Fc fusion protein (BMPR1B-Fc); human platelet-derived growth factor (PDGF)-BB, human TGFβ3, and mouse noggin-Fc fusion protein (noggin-Fc); monoclonal antibodies against collagens type II (COL2, clone 2B1.5) and type X (COL10, clone X53); other staining reagents, and all culture vessels were obtained as described previously (Nakayama et al., 2003; Nakayama et al., 2001). Mouse chordin (mCHD-His); human BMP2, BMP7 and TGFβ1 (and mouse monoclonal antibodies against them); mouse monoclonal anti-human TGFβ3; mouse growth and differentiation factor 5 (GDF5); and affinity-purified goat polyclonal anti-mouse GDF5 were from R&D Systems (Minneapolis, MN). Goat polyclonal anti-human IgG1-Fc fragment (IgG-Fc) was obtained from Sigma. Human kidney epithelial cell lines 293 and 293T were maintained as described previously (Nakayama et al., 2001). The human MSCs (hMSCs) were obtained from BioWhittaker (Walkersville, MD). The E14 mouse ES cells were grown, and embryoid body (EB) cells were harvested, treated and sorted as described previously (Nakayama et al., 2003).

Isolation of mouse, rat and human CHL2 cDNAs

Mouse placentas were isolated at E18. A signal-trap cDNA library and a regular full-length cDNA library were constructed as described previously (Nakayama et al., 2001). From 400 trap-positive clones sequenced, a cDNA fragment encoding the NH_2-terminal sequence of a putative secreted protein with significant homology to *Xenopus* chordin was identified (designated mouse CHL2 or mCHL2) by a BLAST search (Accerlys, San Diego, CA). Using this partial cDNA as a probe, the corresponding full-length cDNA (approximately 1.8 kb) was isolated, and designated as pSPORTmCHL2.

A human placenta library was constructed with size-selected (>1.5 kb) oligo(dT)-primed cDNAs in the pSPORT1 vector (Gibco). A full-length human cDNA clone (hCHL2, 1.5 kb in length) was isolated using the mouse cDNA probe, and designated pSPORThCHL2. Rat CHL2 (rCHL2) cDNA was cloned by PCR from a rat fetal liver cDNA library (Stratagene) using the following primers: sense, 5′-TCCTCTCATCCTCACCTTAG-3′ (based on mCHL2-5′UTR), and antisense, 5′-GAGGGTAATGCGACTTCTTT-3′ (based on mCHL2-3′UTR). A 1.2 kb fragment was amplified using Advantage-HF2 enzyme (Clontech), cloned into pTOPO2.1 (Invitrogen), and designated pTOPOrCHL2.

Production, purification, and detection of recombinant CHL2 protein

To prepare mCHL2, the *mCHL2* open reading frame (ORF) was mutated by PCR to replace the stop codon with a *SalI* site, inserted into a pFLAG-CMV5a expression vector (Sigma) to attach the FLAG sequence in-frame to mCHL2 at its COOH terminus (mCHL2-FLAG), and designated pFLAGmCHL2. Expression was checked by transient transfection of 293T cells, followed by direct western blot analysis of conditioned media, using the anti-FLAG monoclonal antibody M2 as described previously (Nakayama et al., 2001).

A large-scale, transient transfection-based expression was performed as described with 293T cells bearing pFLAGmCHL2 (Nakayama et al., 2001), yielding approximately 10 μg/ml of mCHL2-FLAG. The protein was purified by affinity chromatography using anti-FLAG M2 affinity gel (Sigma) under high-salt conditions, as described by Piccolo et al. (Piccolo et al., 1997), after which positive fractions were subjected to hydroxyapatite column chromatography (equilibrated with 10 mM phosphate, with gradient elution from 10 mM to 400 mM phosphate) at pH 6.9. Purity was confirmed by SDS-polyacrylamide gel electrophoresis followed by Coomassie Blue staining. Approximately 5 mg of >95% pure mCHL2-FLAG protein were obtained from 2.5 l of conditioned medium.

A rabbit polyclonal antibody for mCHL2 (αCHL2-COOH) was raised to the peptide NH_2-CPEDEAEDDHSEVISTR-COOH, and affinity purified against the corresponding peptide (Harlow and Lane, 1988).

Co-immunoprecipitation analysis

Immunoprecipitations to demonstrate direct interactions between BMPs, TGFβs and activin A were performed as described previously (Nakayama et al., 2001) except that only one condition was used: 200 ng mCHL2-FLAG were mixed with 100 ng of BMP/GDF/activin/TGFβ in 1 ml binding buffer, followed by 12 μg/ml of αCHL2-COOH. The BMP/GDF/activin/TGFβ immunocomplex was precipitated with 20 μl protein A agarose beads (Santa Cruz), fractionated on an SDS-polyacrylamide gel (NuPAGE, Invitrogen), blotted, and visualized with the corresponding antibody as described previously (Nakayama et al., 2001), or with 1 μg/ml of anti-BMP2, anti-BMP7, anti-TGFβ1 or anti-TGFβ3 or 0.3 μg/ml of anti-GDF5. Each blot then was treated with 4.4 μg/ml M2 to confirm the precipitation of mCHL2-FLAG. The inhibitory effect of mCHL2-FLAG (0.1-1 μg, in 1 ml binding buffer) on BMP4 binding (at 100 ng/ml) to the BMPR1B ectodomain (BMPR1B-Fc at 1 μg/ml) was performed as described by Nakayama et al. (Nakayama et al., 2001), except that BMP4 visualization on blots was followed by CHL2 and BMPR1B-Fc detection using 4.4 μg/ml M2 and 2.2 μg/ml anti-IgG-Fc, respectively.

Ectopic axis formation in the *Xenopus* embryo

Inhibition of BMP4 by mCHL2 was assessed in *Xenopus* embryos. The *EcoRI-NotI* fragment of pSPORTmCHL2 was cloned into the *EcoRI-NotI* sites of pCS2+ (Rupp et al., 1994), and the resulting plasmid was linearized with *NotI*. Capped mRNAs were synthesized with SP6 polymerase, quantified, diluted and injected into two ventral blastomeres as described previously (Nakayama et al., 2001).

Table 1. Oligonucleotide primers for human genes

Gene		Sequence	Product (bp)
Aggrecan	Sense	5′-ACAGCCACCTCCCCAACAG-3′	414
	Antisense	5′-ATTCCACTCGCCCTTCTCGT-3′	
COMP	Sense	5′-CAGAAGAACGACGACCAAAAG-3′	1000
	Antisense	5′-GCAGGAACCAACGATAGGAC-3′	
COL1	Sense	5′-AGGGCTCCAACGAGATCGAGATCCG-3′	222
	Antisense	5′-TACAGGAAGCAGACAGGGCCAACGTCG-3′	
COL2	Sense	5′-CGTCTACCCCAATCCAGCAAAC-3′	412
	Antisense	5′-GGAGGCGTGAGGTCTTCTGTG-3′	
COL10	Sense	5′-CCAGCAGGAGCAAAGGGAATG-3′	831
	Antisense	5′-GTGGGGTAGAGTTAGAGAATG-3′	
CHL1	Sense	5′-GGGTTGGTTTACTGCGTGAA-3′	647
	Antisense	5′-GACTCGCCATGAGAATAGGTCTT-3′	
CHL2	Sense	5′-TGTGAGTTGTTACCGCCTCCAC-3′	839
	Antisense	5′-GGCTTGGGGATACCGATGTGT-3′	
SOX9	Sense	5′-AGGTAAAAGGCAAGCAAAGGAG-3′	993
	Antisense	5′-CTGGGAGGGAAACAAGTGAAAC-3′	
GAPD	Sense	5′-ACCACAGTCCATGCCATCAC-3′	450
	Antisense	5′-TCCACCACCCTGTTGCTGTA-3′	

Alkaline phosphatase induction in C2C12 cells by BMPs

Promyoblast C2C12 cells were maintained and differentiated according to the method of Kirsch et al. (Kirsch et al., 2000a). Briefly, cells were plated at 3×10^4 cells/well in a 96-well plate, and after 1 day, stimulated to differentiate for 72 hours in 120 μl of Dulbecco's Modified Eagle's medium with 2% calf serum (Gibco) in the presence or absence of BMP and/or CHL2. Cells were washed and lysed. Alkaline phosphatase (AP) activity was measured with *p*-nitrophenyl phosphate (Sigma), with specific activity calculated as the amount of *p*-nitrophenol produced in 30 minutes at 37°C, normalized to total protein content, as determined with BCA reagent (Pierce).

In situ hybridization and northern blot analysis

Northern blotting was performed against the entire open reading frame (ORF) of *CHL2* on human and mouse multiple tissue RNA blots (Clontech) using the ^{32}P-labeled *XbaI-SalI* fragment from pSPORThCHL2 as a probe (Sambrook et al., 1989).

In situ hybridization (ISH) was performed on 5 μm paraffin sections of zinc formalin-fixed, formic acid-decalcified tissue according to the method of Wilcox (Wilcox, 1993), including a high stringency wash with 0.1× SSC at 55°C. Slides hybridized with ^{33}P-labeled RNA probes were exposed to NTB2 emulsion (Kodak) for 3 weeks, developed and counterstained with Hematoxylin and Eosin. Expression was subjectively evaluated under dark-field microscopy.

For *mCHL2*, the 1234-bp *SalI-NotI* fragment and the 653 bp *Hin*dIII fragment were deleted from pSPORTmCHL2 to obtain pSPmCHL2-COOH and pSPmCHL2-NH_2, respectively. Both plasmids were linearized with *Eco*RI to generate non-overlapping probes. An *hCHL2*-bearing plasmid, pSPhCHL2NH2, was made by deleting the 811 bp *Bam*HI fragment from pSPORThCHL2, leaving the 746 bp hCHL2 NH_2-terminal ORF. The plasmid was linearized with *SalI*. RNA probes for *hCHL2* and *mCHL2* were synthesized with SP6 RNA polymerase. For *rCHL2*, an approximately 1.2 kb fragment of rCHL2 cDNA derived from pTOPOrCHL2 was cloned into the pBluescript vector (pBSrCHL2). The plasmid was linearized with *Xba*I and a labeled RNA probe synthesized with T7 RNA polymerase.

CHL2 expression was assessed by ISH in mouse embryonic/adult tissues, and in structurally normal and arthritic joints of adult humans (knee cartilage) and rats (hind paws). Human diseased cartilage samples from rheumatoid arthritis (RA) or osteoarthritis (OA)/degenerative joint disease (DJD) patients were provided by Cooperative Human Tissue Network, and normal control samples were from Zoion Diagnostics (New York, NY), with pre-approval of the Institutional Review Board (758WIRB and CP1098/01, respectively). Collagen-induced arthritis (CIA) was induced, as described (Trentham et al., 1977), in anesthetized female Lewis rats (7-8 weeks old, 150-170 g) by intradermal injection of porcine COL2 (Chrondex, Seattle, WA) emulsified 1:1 in incomplete Freund's adjuvant (Difco, Detroit, MI) at 10 different sites over the back (50 μg COL2/100 μl/injection). Disease developed between 10 and 12 days after injection, as determined by caliper measurements (Cole Parmer, Vernon Hills, IL) of ankle width and ambulatory difficulties. Paws were harvested for ISH 7 days after CIA onset. These experiments were conducted in accordance with federal animal care guidelines and were pre-approved by the Amgen Institutional Animal Care and Use Committee.

Chondrogenic differentiation of MSCs and gene expression analysis

Human MSCs were cultured and differentiated as described (Mackay et al., 1998). Briefly, the pellet culture was performed in serum-free chondrogenesis medium supplemented with 10 ng/ml TGFβ3, with or without 2 μg/ml mCHL2-FLAG, 1 μg/ml noggin-Fc, or 1 μg/ml IgG-Fc. On days 21-28, cartilage-like particles were formalin-fixed, paraffin-embedded, sectioned centrally and stained with Toluidine Blue to detect sulfated glycosaminoglycans (Nakayama et al., 2003; Sheehan and Hrapchak, 1987). Three sections from different regions were examined to confirm staining reproducibility.

To analyze gene expression, two to five particles were harvested at designated times and disrupted immediately in guanidine isothiocyanate solution (RNeasy kit, Qiagen). Total RNA was purified using the manufacturer's protocol, including DNase I treatment. Reverse transcription (RT) and PCR were performed as described previously (Nakayama et al., 1998), except that the PCR used 30 cycles, an annealing temperature of 62°C and one primer set per gene. Primers for aggrecan, cartilage oligomeric matrix protein (COMP), COL1, COL2, COL10, SOX9, CHL1, CHL2 and glyceraldehyde-3-phosphate dehydrogenase (GAPD) are shown in Table 1.

Cartilage mineralization in vitro

Mineralizing cartilage particles were produced as described by Nakayama et al. (Nakayama et al., 2003). Briefly, $3\text{-}4\times10^5$ FACS-purified EB cells were pellet-cultured in serum-free chondrogenesis medium with 10 ng/ml TGFβ3 and 50 ng/ml PDGF-BB. On day 10, TGFβ and PDGF were replaced by 50 ng/ml BMP4 to generate a hyaline cartilage particle. On day 15, cultures were adjusted to the hypertrophic differentiation medium without T3 (Sigma), containing 3 μg/ml mCHL2-FLAG, 2 μg/ml noggin-Fc or 50 ng/ml BMP6 for 3 days; 10 nM T3 was added to induce hypertrophic differentiation on day 18. On days 24-26, each particle was stained with Toluidine Blue as described above (Sheehan and Hrapchak, 1987). Additional serial sections were immunostained with 2B1.5 for COL2 and X53 for

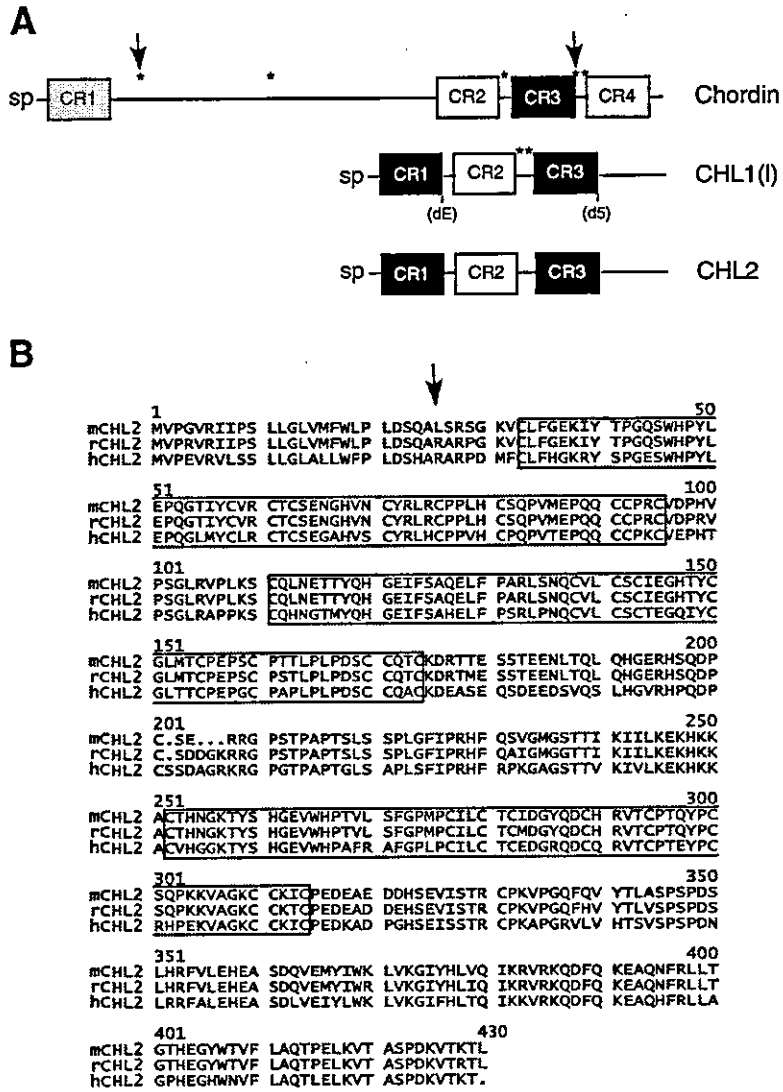

Fig. 1. Primary structure of CHL2. (A) Schematic representation of chordin, CHL1(l), and CHL2. SP stands for signal peptide. The CR1 and CR3 regions in CHL1 and CHL2 (black boxes) are most homologous to CR3 of chordin (also in black). The chordin CR1 (in gray) and CR3 possess the BMP-binding capability (Larrain et al., 2000). Putative BMP1/Tolloid cleavage sites are indicated with an asterisk, while actual Tolloid cleavage sites (Scott et al., 1999) are shown by vertical arrows. The CHL1 ORF had two sites with amino acid sequence variations (dE and d5) (Nakayama et al., 2001). (B) Amino acid sequences of mouse, rat and human CHL2 protein precursors. The three CRs are indicated by boxes. The vertical arrow indicates the NH_2-terminal amino acid of mature mCHL2-FLAG (Leu^{26}), as determined by amino acid sequencing of purified recombinant protein. (C) Amino acid sequence alignment showing sequence similarities between CR1 or CR3 of mouse CHL1 and CHL2, and CR3 of mouse chordin. Ten conserved cysteines (highlighted in black) are found in the spacing typical of vertebrate chordins. Other conserved amino acids are highlighted in gray.

COL10, and stained to reveal mineral deposition (von Kossa). Immunostained sections were counterstained with Gill 2 Hematoxylin, and von Kossa sections with Nuclear Fast Red (Sheehan and Hrapchak, 1987).

Results

Cloning of CHL2, a novel chordin-like gene

Random nucleotide sequencing of a mouse placenta library enriched for genes of secreted and membrane-bound proteins revealed a cDNA encoding a protein precursor consisting of a potential signal peptide followed by three chordin-like cysteine-rich repeat (CRs) homologous to those of chordin and CHL (Fig. 1A,C). A GAP search (Accerlys) revealed amino acid sequence identities with mCHL(l3) and chordin of 41% and 33%, respectively. The predicted precursor size of 426 amino acids resembled mCHL(l3) (448 amino acids) more than mouse chordin (999 amino acids). Because this novel cDNA was clearly homologous to CHL, we designated it CHL2 and renamed CHL as CHL1. Human and rat CHL2 cDNAs were cloned also. The human gene encoded a 429 amino acid precursor with 73% amino acid homology to mCHL2, while the rat variant was 95% identical to mCHL2 (Fig. 1B).

A genomic DNA fragment containing a region spanning at least the 5′-half of *mCHL2* was cloned from a 129SV genomic BAC library (Genome Systems). Using this clone, *mCHL2* was localized to chromosome 7, mapping to a position 66% of the distance from the heterochromatic-euchromatic boundary to the telomere. A search of public genome databases confirmed that *mCHL2* is on 7E1 and *hCHL2* is on 11q13. Therefore, unlike *CHL1*, *CHL2* is an autosomal gene. Interestingly, the exon-intron junctions of *CHL2* were nearly identical to those of *CHL1* (not shown), suggesting that both genes may originate from a common ancestor.

Table 2. Secondary axis formation by CHL2

Type of CHL injected	Embryos with axis duplication/total injected embryos (%)
Uninjected	0/31 (0)
mCHL1(s2)* (10 pg RNA/blastomere)	16/20 (80)
mCHL2 (1 pg RNA/blastomere)	29/39 (74)
mCHL2 (5 pg RNA/blastomere)	27/28 (96)

*pcDNAmCHL(s2) (Nakayama et al., 2001).

MCHL2 induced a secondary axis in the *Xenopus* embryo

Chordin is known to dorsalize the gastrulating *Xenopus* embryo by inhibiting BMP4 activity, so the impact of CHL2 on *Xenopus* embryo development was examined (Table 2). Injection of 1 pg mCHL2 RNA per blastomere induced trunk duplication in 74% of embryos, compared with 0% for uninjected controls and embryos given EF1α mRNA. As a positive control, injection of 10 pg mCHL1(s2) RNA yielded an axis duplication rate of 80% (Nakayama et al., 2001). These results indicated that mCHL2 actively antagonized an endogenous ventralizing factor (presumably BMP4). The improved efficacy afforded by a 10-fold lower CHL2 dose suggested that it might be a more stable and/or potent BMP inhibitor than CHL1.

Direct interaction of mCHL2 with BMPs prevents their binding to BMP receptor

mCHL2-FLAG protein was purified to near homogeneity (Fig. 2A). Unlike mCHL1(s2)-FLAG, the overall yield was higher, and degradation products were not detected.

Purified mCHL2-FLAG co-immunoprecipitated BMP2, BMP4, BMP5, BMP6, BMP7 and GDF5 (Fig. 2B). Like chordin and CHL1, mCHL2-FLAG did not bind activin A, TGFβ1 or TGFβ3. However, unlike CHL1, no interaction between mCHL2-FLAG and TGFβ2 was found. The control protein noggin-Fc exhibited comparable qualitative binding specificity (not shown), suggesting that CHL2 may be a pan-BMP-binding protein like noggin and chordin.

Chordin and CHL1 inhibit BMP activity by blocking their interactions with their receptors. Therefore, we determined whether CHL2 had a similar function by mixing an Fc-fusion protein, incorporating the extracellular domain of BMP receptor 1B (BMPR1B-Fc), with BMP4 and mCHL2-FLAG, followed by precipitation of the BMPR1B-Fc complex with protein A beads. As shown in Fig. 2C, BMP4 co-precipitated specifically with BMPR1B-Fc, but not IgG-Fc, in the absence of mCHL2-FLAG. However, the signal for co-precipitated BMP4 weakened appreciably as increasing amounts of mCHL2-FLAG were added (particularly at 0.3 μg/ml or higher). Co-precipitation of mCHL2-FLAG was not detected. These results suggest that CHL2 acts like chordin and CHL1 to prevent BMP4 interacting with its receptor.

CHL2 inhibits BMP in vitro

Next, we demonstrated that the recombinant mCHL2 inhibited BMP activity by quantifying BMP-dependent AP induction in C2C12 cells. A serially diluted BMP inhibitor [chordin (mCHD-His), mCHL2-FLAG, or noggin-Fc] was mixed with BMP2, BMP4, BMP6 or BMP7 at a concentration corresponding to the EC50 for AP induction in C2C12 cells and then cultured for 3 days. Cell-bound AP activity was then measured (Fig. 3, Table 3). CHL2 inhibited AP induction by all four BMPs. Noggin-Fc and mCHL2-FLAG reproducibly elicited similar, dose-dependent inhibitions of BMP4, with complete suppression occurring at concentrations of 1-3 μg/ml (20-60 nM). The mCHD-His activity was weakest for BMP4; it was approximately fivefold less potent than mCHL2-FLAG. Partially purified mCHL1(s2)-FLAG and mCHD-FLAG (Nakayama et al., 2001) inhibited BMP4 with a potency indistinguishable from that of mCHD-His (not shown). In contrast, both noggin-Fc and mCHD-His displayed weaker inhibitory activities than mCHL2-FLAG toward BMP6 and BMP7. In particular, noggin-Fc was approximately sevenfold less potent on BMP6 than mCHL2-FLAG. Thus, CHL2 inhibits BMP2, BMP4, BMP6 and BMP7 as well as or better than noggin and chordin.

CHL2 mRNA expression in normal cartilage

In mouse embryos, ISH for CHL2 mRNA revealed expression restricted to the surface chondrocytes of developing joint cartilage (Fig. 4) and to the connective tissue of reproductive organs (Fig. 5). In the adult mouse, *CHL2* was weakly expressed in cartilage of the femoral head and patella (Fig. 4C,D) and articular facets of vertebrae (Fig. 4E,F); the latter

Table 3. Inhibition of BMP action by CHL2, noggin and chordin

BMP	EC50±s.d. BMP‡ (nM)	IC50*±s.d. mCHL2§ (nM)	IC50†±s.d. mCHL2 (nM)	IC50†±s.d. noggin¶ (nM)	IC50†±s.d. chordin** (nM)
BMP2	14.2±4.6 (*n*=14)	4.1±1.7 (*n*=6)	ND††	ND	ND
BMP4	10.0±3.5 (*n*=16)	5.0±1.5 (*n*=6)	3.0±0.9 (*n*=12)	3.6±0.6 (*n*=5)	15.4±2.2 (*n*=7)
BMP6	15.0±4.3 (*n*=12)	5.8±3.0 (*n*=7)	5.2±2.2 (*n*=3)	34.6±16.6 (*n*=2)	10.3±4.9 (*n*=2)
BMP7	33.4±5.4 (*n*=8)	12.5±2.6 (*n*=5)	3.2±1.1 (*n*=3)	9.4±3.0 (*n*=2)	7.4±1.8 (*n*=2)

C2C12 cells were cultured for 3 days with various BMP concentrations or with a fixed BMP level and various quantities of CHL2, chordin or noggin. Alkaline phosphatase activities were measured, normalized to total protein level, and plotted to determine EC50s and IC50s. Mean values (±s.d..) of 2-16 experiments (*n*=2-16), are shown.

*BMP2: 14 nM, BMP4: 10 nM, BMP6: 15 nM, BMP7: 25 nM.

†BMP4: 4-7.7 nM, BMP6: 13 nM, BMP7: 19 nM (Fig. 3).

‡BMP2: 26 kD, BMP4: 26 kD, BMP6: 30 kD, BMP7: 31.4 kD, as dimer (R&D).

§mCHL2-FLAG: mature peptide, 46.5 kD (415 amino acids) as monomer.

¶noggin-Fc: 50 kD as monomer (R&D).

**mCHD-His: 101.5 kD as monomer (R&D).

††Not determined.

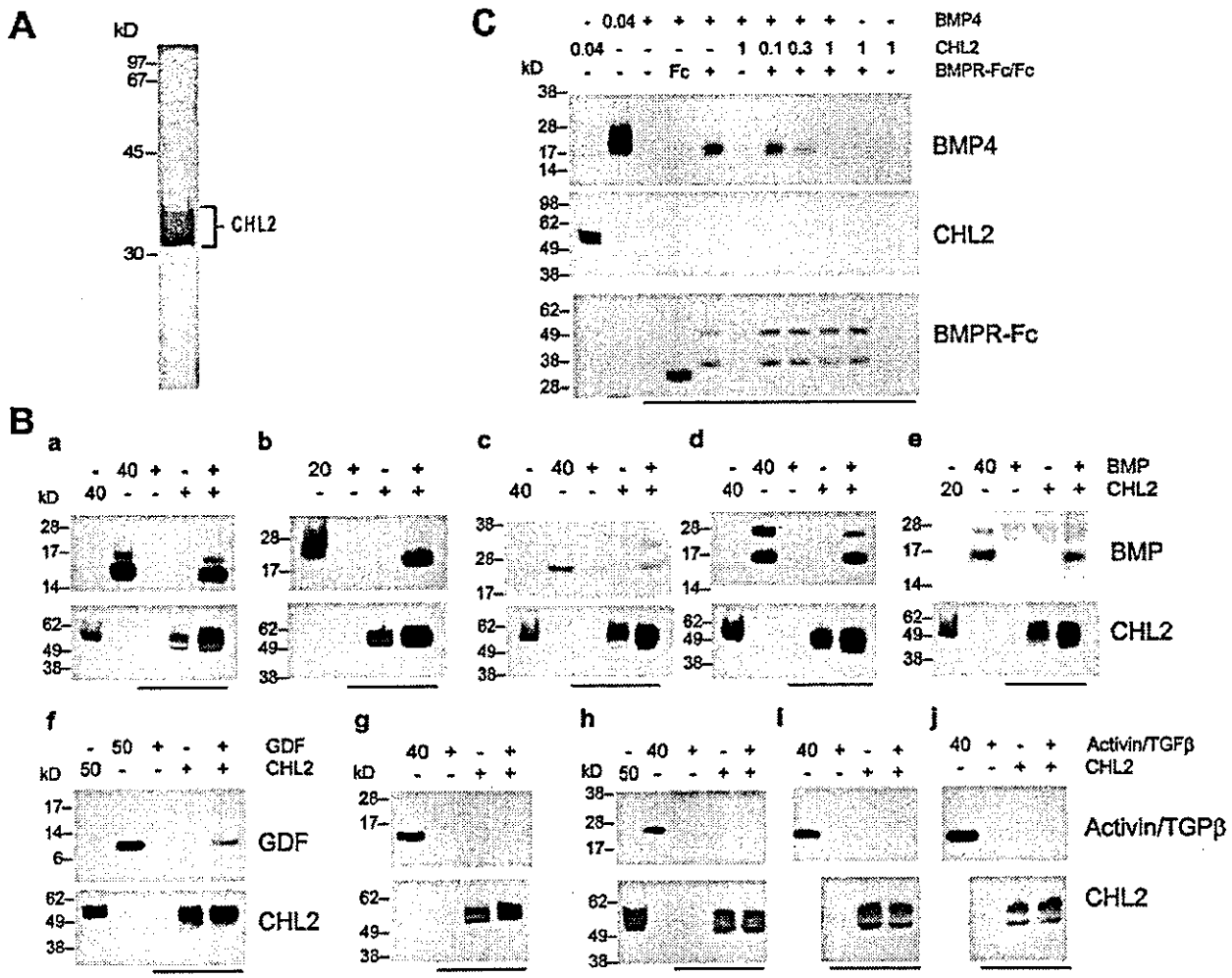

Fig. 2. Direct interaction of mCHL2 with BMPs, and inhibition of BMP4 binding to BMP receptor ectodomain by mCHL2. (A) FLAG-tagged CHL2 protein. Proteins in the peak eluate from the hydroxyapatite column chromatography were separated by SDS-polyacrylamide gel electrophoresis under reducing conditions and then silver stained (Sambrook et al., 1989). The mCHL2-FLAG band was excised and the NH_2-terminal amino acid sequence (vertical arrow in Fig. 1B) determined. (B) Immunoprecipitation/western blot analysis of mCHL2-FLAG individually mixed with BMP2 (a), BMP4 (b), BMP5 (c), BMP6 (d), BMP7 (e), GDF5 (f), activin A (g), TGFβ1 (h), TGFβ2 (i) or TGFβ3 (j), followed by treatment with αCHL2-COOH (lanes underlined). Immunocomplexes were detected using the corresponding antibodies (upper panels). Reactions only with mCHL2-FLAG, BMP, GDF, activin or TGFβ were also performed as negative controls. Each blot was further developed with M2 to confirm the presence of precipitated mCHL2-FLAG (lower panels). The TGFβ immunocomplexes (h-j) were separated into two sets; one was loaded on a non-reducing gel to visualize TGFβ (upper panels), and the other on a reducing gel to detect CHL2 (lower panels). Lanes not underlined were directly loaded with the indicated amount (ng) of mCHL2-FLAG, BMP, GDF, activin or TGFβ (for standards). (C) Inhibition of BMP4 binding to BMPR1B ectodomain by mCHL2-FLAG. The indicated amount of mCHL2-FLAG was first mixed with or without BMP4, and then BMPR1B-Fc or IgG-Fc was added. Protein complexes containing BMPR1B-Fc or IgG-Fc were selectively precipitated with protein A and subjected to western blot analysis (lanes underlined). Upper panel: bound BMP4 visualized with anti-BMP4 antibody. Middle panel: co-precipitation of mCHL2-FLAG checked with M2. Lower panel: precipitation of BMPR1B-Fc/IgG-Fc confirmed with anti-IgG-Fc antibody. For the standards, 0.04 μg of mCHL2-FLAG and 0.04 μg of BMP4 were loaded directly.

location had a relatively stronger signal. *CHL2* was also expressed weakly in the annulus fibrosus of intervertebral discs in adults (not shown). In general, *CHL2* expression in adult cartilage was weaker than that of embryonic cartilage. *CHL2* in normal cartilage was confined to articular chondrocytes, especially in the superficial zone. Expression was always observed on both sides of a joint. CHL2 transcripts were never detected in growth plate cartilage or bone during development or adulthood. In rats, *CHL2* also showed low to moderate expression in sternal cartilage during embryogenesis (not shown) and in joint cartilages of adult paws (Fig. 6). Thus, among skeletal compartments, *CHL2* seems to be expressed preferentially in the superficial zone chondrocytes of developing articular cartilage.

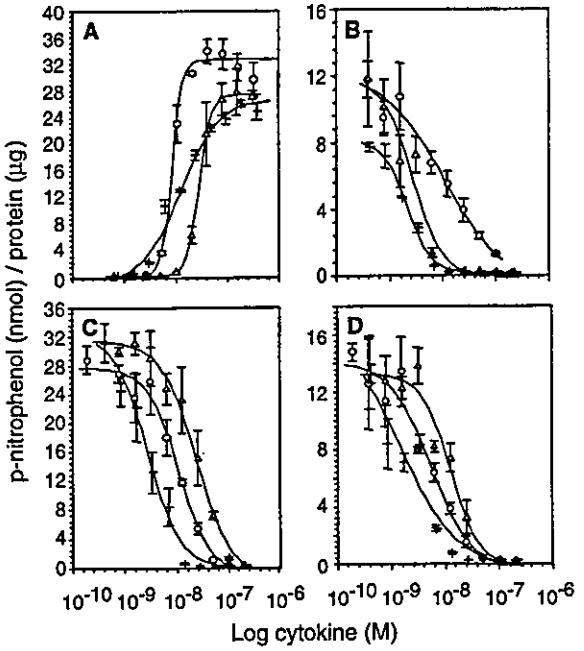

Fig. 3. Inhibitory effects of mCHL2 on BMP-dependent differentiation of C2C12 cells in vitro. Dose-dependent inhibition by CHL2, chordin or noggin of BMP-dependent alkaline phosphatase (AP) induction in C2C12 cells. (A) Cells were cultured in differentiation medium for 2 days with various concentrations of BMP4 (plus sign), BMP6 (circle), or BMP7 (triangle). (B-D) Cells were also differentiated with a constant concentration of BMP4 (10 nM; B), BMP6 (15 nM; C) or BMP7 (19 nM; D) and various concentrations of mCHL2-FLAG (plus sign), noggin-Fc (triangle), or mCHD-His (circle) for 2 days. Mean specific activity of AP (triplicate assays) is shown; vertical bars denote s.d. Data are representative of three independent experiments.

Normal, non-skeletal expression of the CHL2 gene

Northern analyses revealed little mCHL2 mRNA on the mouse embryo blot, in contrast to the abundant expression of mouse chordin and mouse CHL1 (Nakayama et al., 2001). On the mouse adult tissue blot, a faint 2 kb transcript was detected in liver and kidney extracts, and a trace amount of a >2.4 kb transcript was detected in skeletal muscle and testis, although ISH failed to localize a signal in these tissues (not shown). The adult mouse blot did not include uterus. On the human adult tissue blot, a 2 kb CHL2 transcript was detected readily in uterus and weakly in colon, heart, prostate, stomach and skeletal muscle (Fig. 5A); only the uterus and colon had expression patterns consistent with the ISH signals in mouse tissues (Fig. 5B). Traces of hCHL2 mRNA were found in placenta, testis, small intestine, trachea and bone marrow. Expression was not detected in either human liver or kidney. Thus, low levels of *CHL2* expression in soft tissues may differ between humans and mice.

In mouse reproductive organs, ISH detected CHL2-positive connective tissues such as ligaments of the ovary and oviduct in females, and of testis, epididymis and certain male accessory sex glands in males. Expression was high in uterine myometrium (Fig. 5Ba), as was that of CHL1 (not shown). CHL2 was also present in maternally derived placental tissues (not shown). A trace CHL2 signal was found on colonic serosa (Fig. 5Bb); in contrast, CHL1-positive cells lie between the colonic submucosa and muscularis (Nakayama et al., 2001). Interestingly, *CHL1* but not *CHL2* was expressed in stomach and small intestine (Nakayama et al., 2001). In rat tissues, CHL2 occurred at low to moderate levels in cervical muscles and discrete regions of the placenta (not shown).

CHL2 mRNA expression in diseased cartilage

Degenerating cartilage from human arthritis patients and rats with CIA were assessed by ISH (Fig. 6). In two relatively normal specimens from knees of adult humans, CHL2 mRNA was expressed in a few chondrocytes in the superficial zone as well as in the middle zone (Fig. 6A). In 19 OA cases, expression was limited to chondrocytes in the middle zone, where numerous well-labeled cells were observed (Fig. 6B,C); positive cells were not found in the superficial zone in any OA sample. Interestingly, 50-90% of such *CHL2*-expressing chondrocytes existed in clusters of 2-3 cells. Unlike OA, two RA specimens exhibited weak expression in both the superficial and middle zones (Fig. 6D). As with humans, scattered chondrocytes in normal articular cartilage of rats expressed *CHL2* (Fig. 6E), while CIA paw joints had similar (Fig. 6F) or fewer labeled chondrocytes relative to controls.

In summary, *CHL2* was expressed in normal and diseased cartilage in humans and rats. It was expressed most strongly in human OA patients, although the signal had shifted to the middle zone. Interestingly, *CHL2* expression levels and patterns were not significantly altered, relative to normal cartilage, in the rat CIA model and human patients with RA.

Effects of CHL2 on MSC differentiation into chondrocytes

We further addressed the relevance of CHL2 to cartilage formation using MSC, which can differentiate into chondrocytes in vitro (Mackay et al., 1998) in association with upregulated BMP transcription (Roh et al., 2001). As shown by RT-PCR in Fig. 7A, hCHL2 mRNA, but not COL2 mRNA, was expressed by undifferentiated MSCs. Transcripts for SOX9, COL1 and COL10 (not shown) as well as CHL1, aggrecan and COMP were also detected. The CHL2 signal fell as chondrogenesis progressed; those for SOX9 and COL10 (not shown) as well as CHL1, aggrecan and COMP (Fig. 7A) maintained a similar level throughout the culture period. In contrast, COL2 mRNA was tightly regulated, with production induced by day 7 in culture conditions favoring chondrogenesis but absent under osteogenic conditions (not shown) (Jaiswal et al., 1997).

Next, mCHL2-FLAG protein was added at various concentrations to the chondrogenic pellet culture of MSC. mCHL2-FLAG (2 µg/ml) significantly inhibited cartilage nodule formation (Fig. 7B, Table 4), yielding definitive cartilage nodules in less than 10% of particles. Inhibition was absent at 0.1-0.2 µg/ml, while complete inhibition occurred at 3-10 µg/ml. Noggin-Fc at 0.1 and 1 µg/ml provided similar, dose-dependent inhibition.

These results implicate CHL2 as a negative regulator of cartilage formation/regeneration from immature mesenchymal cells, by preventing or reducing the rate of matrix accumulation.

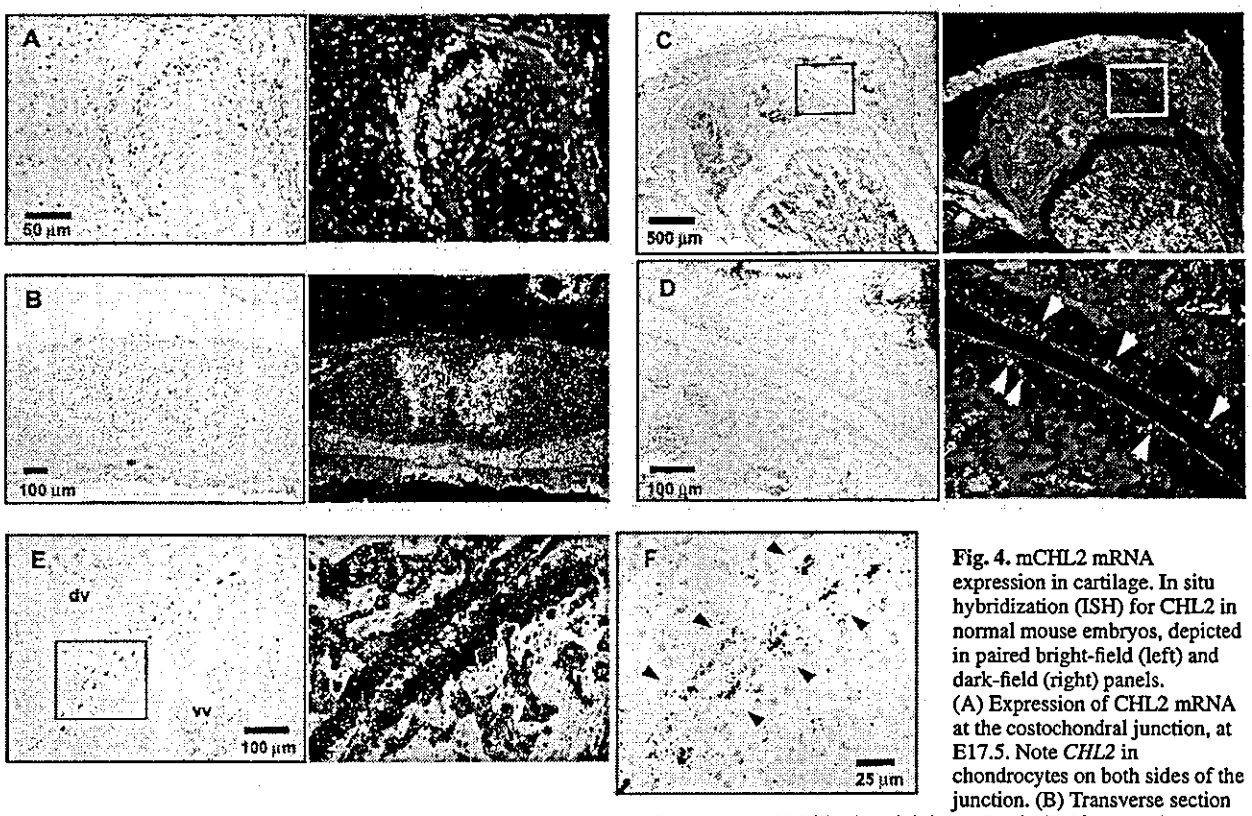

Fig. 4. mCHL2 mRNA expression in cartilage. In situ hybridization (ISH) for CHL2 in normal mouse embryos, depicted in paired bright-field (left) and dark-field (right) panels. (A) Expression of CHL2 mRNA at the costochondral junction, at E17.5. Note *CHL2* in chondrocytes on both sides of the junction. (B) Transverse section through sternum, at E18.5. Signal is present in areas where ribs converge. (C,D) ISH for *CHL2* in the adult knee. Weak *CHL2* expression is present over the articular cartilage surface of the femoral head and patella, but not in growth plate chondrocytes. Boxed areas in C shown at a higher magnification in D in which the signal can be seen in chondrocytes on both sides of the joint. (E,F) Expression of *CHL2* in adult vertebral articulation. Signal occurs in superficial articular chondrocytes on both sides of the zygapophyseal or facet joint. The boxed area in E is shown at a higher magnification in F, revealing signal localization over the superficial zone chondrocytes. dv, dorsal (superior) vertebra; vv, ventral (inferior) vertebra. Arrowheads indicate CHL2-positive chondrocytes.

Table 4. Inhibition of cartilage-matrix deposition by CHL2

Factors*	Cartilaginous particles† (% total)	Weak-positive particles‡ (% total)	Negative particles§ (% total)
TGFβ3	20 (87.0)	3 (13.0)	0 (0)
TGFβ3+noggin-Fc	2 (18.2)	2 (18.2)	7 (63.6)
TGFβ3+mCHL2-FLAG	1 (6.7)	3 (20.0)	11 (73.3)

Human mesenchymal progenitor cells, cultured as a pellet for 21-28 days, were fixed, sectioned and stained with Toluidine Blue. Particles were classified on the basis of their degree of metachromatic staining.

*10 ng/ml TGFβ3, 1 μg/ml (20 nM) noggin-Fc, 2 μg/ml (43 nM) mCHL2-FLAG.

†Particles containing definitive cartilage nodules, consisting of well-separated chondrocytes embedded in proteoglycan-rich extracellular matrix (with metachromatic Toluidine Blue staining and positive Alcian Blue staining, pH 1.0) (Fig. 7Ba,b,d,e). These particles also contained regions with fusiform cells that stained lightly with Toluidine Blue (Fig. 7Bb,d).

‡Particles consisting of Toluidine Blue-negative cells as well as relatively larger areas of fusiform cells that stained lightly with Toluidine Blue. The latter areas occasionally contained a small cartilaginous nodule, consisting of a few chondrocytes, as shown in Fig. 7Bf.

§Particles containing no cartilage nodules, but instead with a surface layer of spindle-shaped cells that stained lightly with Toluidine Blue, as shown in Fig. 7Bc.

Effects of CHL2 on chondrocyte maturation

Chondrocytes from OA joints express markers of hypertrophy, such as COL10 and AP (Kirsch et al., 2000b; Von der Mark et al., 1992), so we addressed whether CHL2 induction in OA cartilage would affect differentiation and mineralization of hypertrophic chondrocytes. We demonstrated previously that mesodermal progenitor cells, purified from differentiating ES cells, can form hyaline cartilage particles in vitro that will undergo further mineralization (Nakayama et al., 2003). We isolated FLK1$^-$ PDGFRα$^+$ mesodermal cells, subjected them to pellet micromass culture, and induced cartilage matrix mineralization (verified by von Kossa staining) in the presence or absence of mCHL2-FLAG, noggin-Fc or BMP6 (Fig. 7C, Table 5). Addition of 3 μg/ml mCHL2-FLAG significantly reduced the von Kossa-positive matrix area in 75% of particles examined, of which half showed near-complete inhibition. In contrast, COL10 expression was reduced slightly, while no significant change was detected in COL2 (Fig. 7C). Noggin-Fc at 2-3 μg/ml provided similar, but somewhat weaker, inhibition. A positive in vitro role for BMP6 has been suggested in chondrocyte hypertrophic differentiation (Grimsrud et al., 1999). However, BMP6 at 50 ng/ml, which